



## **Deep mass redistribution prior to the 2010 Mw 8.8 Maule (Chile) Earthquake revealed by GRACE satellite gravity**

Marie Bouih, Isabelle Panet, Dominique Remy, Laurent Longuevergne, Sylvain Bonvalot

### **► To cite this version:**

Marie Bouih, Isabelle Panet, Dominique Remy, Laurent Longuevergne, Sylvain Bonvalot. Deep mass redistribution prior to the 2010 Mw 8.8 Maule (Chile) Earthquake revealed by GRACE satellite gravity. *Earth and Planetary Science Letters*, 2022, 584, pp.117465. <10.1016/j.epsl.2022.117465>. <insu-03609882>

**HAL Id: insu-03609882**

**<https://insu.hal.science/insu-03609882v1>**

Submitted on 16 Mar 2022

**HAL** is a multi-disciplinary open access archive for the deposit and dissemination of scientific research documents, whether they are published or not. The documents may come from teaching and research institutions in France or abroad, or from public or private research centers.

L'archive ouverte pluridisciplinaire **HAL**, est destinée au dépôt et à la diffusion de documents scientifiques de niveau recherche, publiés ou non, émanant des établissements d'enseignement et de recherche français ou étrangers, des laboratoires publics ou privés.



HAL Authorization

# Deep mass redistribution prior to the Mw 8.8 Maule Earthquake (Chile) revealed by GRACE satellite gravity

Marie Bouih (1), Isabelle Panet (1,2), Dominique Remy (3), Laurent Longuevergne (4),  
Sylvain Bonvalot (3)

(1) Université de Paris, Institut de physique du globe de Paris, CNRS, IGN, F-75005 Paris, France

(2) ENSG-Géomatique, IGN, F-77455 Marne-la-Vallée, France

(3) GET, Université de Toulouse, IRD, UMR 5563 CNRS, CNES, Toulouse, France

(4) Univ Rennes, CNRS, Geosciences Rennes - UMR 6118, F-35000 Rennes, France

Corresponding author: Marie Bouih (bouih@ipgp.fr)

## Abstract

Subduction zones megathrust faults constitute a considerable hazard as they produce most of the world's largest earthquakes. However, the role in megathrust earthquake generation exerted by deeper subduction processes remains poorly understood. Here, we analyze the 2003 – 2014 space-time variations of the Earth's gravity gradients derived from three datasets of GRACE geoid models over a large region surrounding the rupture zone of the Mw 8.8 2010 Maule earthquake. In all these datasets, our analysis reveals a large-amplitude gravity gradient signal, progressively increasing in the three months before the earthquake, North of the epicentral area. We show that such signals **are equivalent to a 60 km<sup>3</sup> water storage decrease over 2 months and** cannot be explained by hydrological sources nor artefacts, but rather find origin from mass redistributions within the solid Earth on the continental side of the subduction zone. These gravity gradient variations



26 could be explained by an extensional deformation of the slab around 150-km depth along  
27 the Nazca Plate subduction direction, associated with large-scale fluid release. Further-  
28 more, the lateral migration of the gravity signal towards the surface from a low coupling  
29 segment around  $-32.5^\circ$  North to the high coupling one in the South suggests that the  
30 Mw 8.8 Maule earthquake may have originated from the propagation up to the trench of  
31 this deeper slab deformation. Our results highlight the importance of observations of the  
32 Earth's time-varying gravity field from satellites in order to probe slow mass redistributions  
33 in-depth major plate boundaries and provide new information on dynamic processes in the  
34 subduction system, essential to better understand the seismic cycle as a whole.

35

## 36 **Keywords**

37 Gravity gradients, GRACE, Earthquake, **Signal separation**

# 1 Introduction

The February 27<sup>th</sup>, 2010,  $M_w$  8.8 Maule earthquake is one of the largest ~~instrumental~~ earthquakes **instrumentally recorded earthquakes**. It nucleated in the central region of the historic 1835 Concepcion event ( $M_w$  8.5), matching a zone of high coupling previously characterized as a mature seismic gap [41]. This event ruptured a 500-km length segment of the interface between the downgoing Nazca and the over-riding South American plates, releasing stresses accumulated over more than 175 years since the last  $M_w$  9 earthquakes in 1730 and 1751 [48]. It produced up to 7-12 meters of thrust slip in the 24-35km depth range. The largest slip ( $\sim 16$ m) was found in the northern portion of the ruptured zone, where a  $M_w$  7.7 earthquake occurred in 1928 [22] [33].

The slip distribution of the 2010 Maule earthquake has been derived from seismological records [22], tsunami data and space geodetic observations [27][11]. While the seismological data are sensitive to the propagation of the rupture during the event, space geodesy detects the surface motions offsets after the rupture and their slow post-seismic variations, continuously over years or decades in the case of the ~~GNSS~~ **Global Navigation Satellite Systems (GNSS)**. Based on these two types of observations, the earthquake slip distribution is however not fully constrained at depth (e.g. [25]) and the post-seismic deformation processes remain debated, from localized afterslip in the seismogenic zone to viscous flow in the mantle. Ambiguities result in particular from a limited spatial distribution of the ground stations, mostly on land, and an imperfect knowledge of material properties of the Earth.

At medium spatial scales, co-seismic and post-seismic mass redistributions have been detected by the Gravity Recovery and Climate Experiment (GRACE) satellites. This mission measured the space-time variations of the Earth's gravity field with a decadal to monthly temporal resolution and 250-400km spatial resolution from 2002 to 2017 [47]. As for other giant ruptures monitored by GRACE, a co-seismic dipole marked by a predomi-

nant gravity decrease on the continental side of the subduction was observed for the Mw 8.8 Maule earthquake [17] [15] [9]. It was followed by ~~shorter and long-term post-seismic~~ **long- and short-term post-seismic** signals featuring a slow gravity increase around the trench [46] [8]. The homogeneous spatial coverage of satellite gravity provided key additional information in order to constrain the geometric parameters of the ruptured fault and its average slip [49] [9] and to discuss the nature of the post-seismic processes [46] [15].

Recently, regional-scale gravity variations have been detected in the GRACE geoids in the months before the giant rupture of the March 2011 Mw 9.1 Tohoku-Oki earthquake. They have been attributed to slab deformation at mid-upper mantle depth, eventually leading to the seismic slip as the deeper motion propagated towards the surface [36]. These results have been corroborated by independent GNSS data exhibiting regional crustal deformations of a few millimeters from October 2010 to March 2011, which have been related to slab extension prior to the earthquake, near 50-100km depth [2]. Thus, geodesy and gravity open new ways to analyze the subduction process from depth to surface, including the occurrence of giant ruptures. The unique sensitivity of satellite gravity to deeper mass redistributions offered an information complementary to the surface displacements in order to monitor aseismic motions at all depths in the subduction system.

Deciphering these tenuous solid Earth signals in the gravity field variations however requires to resolve a separation challenge: the GRACE data integrate the total gravity change induced by all the mass variations within the near-surface fluid layer and the solid Earth. We need to decipher the signals from different sources such as hydrological, atmospheric and oceanic mass variability or viscoelastic Earth deformation from post-glacial rebound [4] [35], predominant in the total gravity signal. This is a major challenge in the application of satellite gravity data to track deeper deformations, calling for dedicated analysis techniques. To solve this separation challenge, we will analyze horizontal gravity gradients rather than the geoid. Indeed, gravity gradients help identify a source from the spatial shape of its gravity signal, which is finely described thanks to the double differ-

entiation of the gravity potential [36]. This way we can unravel smaller signals if their geometry differs from that of the predominant ones.

Here, we investigate whether anomalous gravity variations preceding the 2010 Maule event can be detected in the GRACE data. We consider a broad space-time window around the earthquake, from January 2003 to July 2014 in a  $90^\circ \times 120^\circ$  wide region around Central Chile. We first analyze different sets of GRACE gravity field models to search for abnormal signals before the rupture. For that, we enhance small gravity variations using gravitational gradients reconstructed from GRACE at different spatial scales. Then, we evaluate the obtained signals with respect to independent estimations of water storage changes by hydrological models and in-situ observations. This analysis allows us to propose and discuss a deeper origin inside the solid Earth, involving slab deformations near 150-km depth prior to the rupture.

## 2 Data and methods

### 2.1 GRACE geoid models

To search for gravity signals associated to the Maule earthquake in the South American subduction system, we apply a space-time analysis of the time series of the GRACE geoid models over the January 2003-September 2014 period. To assess the sensitivity of the signals to the North-South oriented striping noise that degrades the GRACE geoids, we considered three sets of geoid models obtained by different groups, provided in the form of spherical harmonics expansions: the CNES/GRGS Release 3v1 (GRGS) up to degree/order 80 [24], the ITSG-2016 solution up to degree/order 90 [30] and the CSR Release-06 solution (CSR) up to degree/order 90 [42]. the CSR Release-06 solution (CSR) up to degree/order 60 [42] and the ITSG-2016 solution up to degree/order 60 [30]. For the studied area at the beginning of 2010, we indeed found less striping in the North-South gravity

gradients in the ITSG-2016 solution as compared to the ~~more recent~~ ITSG-2018 release. Due to a different analysis of the GRACE observations, the ITSG-2016 and CSR gravity models show a higher level of striping artefacts than the GRGS solution. To minimize ~~the striping~~ these artefacts in these last two fields, we truncated their spherical harmonics expansion at the degree and order 40. We have verified that at this 500-km resolution, the signal-to-noise ratio remains favourable.

## 2.2 Hydrological models and in-situ data

Separation of solid Earth and hydrological signals is based on both a model-driven and a data-driven approaches. We considered an ensemble of four complementary hydrological models: 1. GLDAS NOAH 2.1 land surface model [39], 2. WGHM global hydrological model [34], 3. ERA5-Land land surface model [10] and 4. the regional MGB model for South America [44]. For comparison with the GRACE observations, we reconstructed each month the geoid and the gravity gradients predicted by these different models, considering the direct newtonian attraction of the water loads and applying a thin layer approximation. In specific regions, we estimate water storage changes from in-situ observations: river discharge (Q) provided by the Global Runoff Data Centre (GRDC), precipitation (P) from the Global Precipitation Climatology Center (GPCC) [43] and actual evapotranspiration (E) provided by the Max Planck Institute [21] (see Appendix E for a more detailed description of the used datasets).

~~To separate solid Earth and hydrological signals, we designed both a model-driven and a data-driven approach to define the impact of water redistribution on gravity. We considered four complementary hydrological models: 1. The global GLDAS NOAH 2.1 model (including soil moisture, snow and water stored in the canopy) at 0.25° resolution [39], 2. the global WGHM model (including soil moisture, snow, groundwater and surface water) at 0.5° resolution [34], 3. the global ERA5-Land model at 9-km resolution (including soil moisture and snow) [10] and 4. the regional MGB model for South America (including canopy, soil moisture, ground water and surface water) at 10-km resolution [44]. We~~

reconstructed each month the geoid and the gravity gradients predicted by these different models, considering the direct newtonian attraction of the water loads and applying a thin layer approximation. Here, the model ensemble is used to better quantify errors arising from forcing data, model structure, and model spatial resolution.

In specific regions, we complete the model analysis with water storage changes inferred from in-situ observations. We considered observations of river discharge (Q), precipitation (P) and actual evapotranspiration (E). The precipitation is based on the Global Precipitation Climatology Center (GPCC) “Full Data Monthly Version 2020” dataset [43]. The GPCC provides gridded gauge-analysis products derived from quality controlled station data, at  $0.25^\circ$  resolution [40]. The actual evapotranspiration is provided by the Max Planck Institute [21]. It is estimated from a data-driven approach, based on a global monitoring network, meteorological and remote-sensing observations, and a machine-learning algorithm. Finally, we used river discharge data and basin outlines provided by the Global Runoff Data Centre (GRDC). The hydrological analysis is performed over 2005-2012 when discharge data is available, in order to remove properly annual and semi-annual signals. Furthermore, in order to remove the potential impact of systematic bias in the fluxes data (e.g. [26]), a linear trend is fitted on water storage changes over the 2005-2012 period.

## 2.3 Gravity gradients at different spatial scales

In order To separate signals associated with **from** mass sources of different sizes, shapes or orientations in the GRACE geoids, we reconstruct each month from these geoid models the Earth’s gravity gradients at different spatial scales, expressed in spherical frames: 1) the distinction between signals of different sizes is made by a wavelet analysis of the GRACE gravity potential [18]; 2) the source geometry is emphasized by computing **horizontal** gravity gradients. In cartesian coordinates, these **gravity** gradients result from a double differentiation of the wavelet-filtered gravity potential with respect to the three

directions of space [35]; then they are expressed at each point in the local spherical frame through appropriate coordinate transformations. As they highlight gravity signals **elongated** orthogonal to the differentiation direction, the ~~obtained~~ **horizontal** gradients provide us with a detailed description of the geometry of the gravity field variations at each spatial scale, reflecting the structure and spatial extent of the sources (Appendix Fig. S1). From a general point of view, rotating the spherical frame along the radial axis is well-suited to separate gravity variations along the orientation of a subduction zone which could be potentially related to an earthquake, from water mass redistribution signals following other orientations. As both GRACE noise and the South-American subduction zone follow a North-South orientation, we average the gradients over a range of orientation ( $\phi$  gravity gradients from  $-10$  to  $10^\circ$  clockwise spherical frame rotations) around the North-South direction to increase signal-to-noise ratio, and we used directions close to East-West, orthogonal to the GRACE noise. The same methodology is applied to hydrological models.

## 2.4 Piece-wise linear fit of anomalous signals

We then analyze the time series of gravity gradients at the different scales and in the different orientations, in order to search for anomalously large gravity variations before the Maule earthquake and compare them with the consecutive co-seismic signals. We first estimate and remove from the time series annual and semi-annual sinusoidal terms accounting for the seasonal variability and a long-term trend, all estimated over the 2003/01-2008/12 period to limit the potential impact of a precursor, and apply the correction to the whole time series. Then, we analyze the residual time series  $g(t)$  as follows:

- We perform a piece-wise linear fit [36] of the time series  $g(t)$  with a free jump in March 2010, which is the first month actually recording the co-seismic step in the GRACE data (Appendix Fig. S2). For that, we decompose the time series of gravity gradients into four consecutive segments separated by a free step in March 2010: [January 2003 -  $t_1$ ], [ $t_1$  - February 2010], [March 2010 -  $t_2$ ] and [ $t_2$  - September 2014] with  $t_1$  = July 2009 and  $t_2$  =

March 2011. The first interval is the reference before the earthquake. The second interval represents the variations in the months preceding the earthquake, potentially including a fast pre-seismic signal. It is fixed to 8 months as a compromise between a too short interval (for which the trend estimate would be very sensitive to noise) and a too long one (for which the meaning of a sudden pre-seismic gravity variation would be lost). **Actually, our conclusions do not change when we vary the length of this interval between 1 and 8 months.** The free jump in March 2010 highlights the co-seismic signal. For the two last intervals, we take  $t_2$  equal to March 2011. This way, we account for variations of the post-seismic gravity signals between the first year and the rest of the time series.

- Anomalous variations before the earthquake are identified by the combination of 1. a large trend ( $>0.1$  mEötvös) over the 8 months interval preceding the rupture in the piece-wise linear fit, together with 2. an abnormal gravity gradient signal in the month before the earthquake (February 2010), marked by a very low probability of occurrence in the observations ( $\geq 5\sigma$ , i.e. probability below  $2.5 \cdot 10^{-6}\%$ ). To detect these abnormal variations in the monthly gravity gradients, we assume that the time series of residuals  $g(t)$  follow a Gaussian distribution and calculate its parameters, at each spatial grid point, over the reference period 2003/01-2008/12. This way we detect anomalous signals before the rupture, both in the February 2010 monthly snapshot and at a timescale of a few months, without making any hypothesis on the behaviour of the rest of the time series after February 2010 (such as the occurrence of a co-seismic variation). This approach allows us to detect a large and monotonous variation progressively realized over a few months, which culminates in highly abnormal values at the end of the considered period.

- We search for the co-seismic signal, identified by the combination of 1. a large jump in March 2010 in the piece-wise linear fit, together with 2. an abnormal gravity gradient signal in March 2010 (probability below  $2.5 \cdot 10^{-6} \%$ ), and 3. a shift in the distribution of the residual time series  $g(t)$  after the earthquake as compared to the years before, indicating some degree of persistence over time of the co-seismic jump (“step-like” temporal



variation). This last criterium is simply implemented by a threshold in the amplitude of a Heaviside function centered at the time of the earthquake.

This method enables us to make a clear distinction between fast variations right before the rupture and the co-seismic variation itself. The co-seismic amplitude is given by the jump in the piece-wise linear fit, while the linear trends after the rupture can approximate faster and slower post-seismic signals. ~~Over these relatively short post-seismic time intervals, exponential and logarithmic behaviors, as may be expected in the presence of afterslip or visco-elastic deformations, can be approximated by linear evolution [19].~~ Fitting the post-seismic behavior is required to better estimate the pre- and co-seismic signals but remains beyond the scope of the paper.

## 3 Results

### 3.1 Slow to fast gravity jumps near the epicenter

We present here the results obtained for an analysis scale of 800-km, commensurate with the rupture length. At larger spatial scales, the earthquake signals progressively decay as the scales become too large as compared to the spatial extent of the signal. The smallest spatial scale that can be reached (500-km) given the resolution of the GRACE geoids is presented in the Section 4.2.1.

Around the epicenter, the two-lobe gravity signal confirms the impact of the co-seismic jump during the month of March 2010 (Fig. 1b, zoomed in Fig. 1d) that was observed in previous studies. It comprises a negative gravity gradient anomaly over the ocean and a positive one over the continent with amplitudes up to 0.19 mEötvös, persistent in the consecutive years. For comparison, the co-seismic gravity gradient signature of the 2011 Tohoku earthquake is twice larger at this spatial scale. Furthermore, we find that this co-seismic variation is preceded by an anomalously large gravity gradient increase in the

months before the rupture, located North of the epicentral area (Fig. 1a, zoomed in Fig. 1e)(Fig. 1a,c). It stands out as the most abnormal signal over the entire South American continent, manifested by the most widespread February 2010 anomaly. This signal exceeds the  $5\sigma$  level of the long-term distribution, after a large increase over 8 months. Thus, among all the medium-scale gravity variations in the months before the earthquake, the largest one is the closest to the epicenter. It is also detected in the wavelet-filtered geoid, although less well separated from neighbouring hydrological sources (Appendix B).

These variations are reflected in time series of the gravity gradients at different locations within these signals (Fig. 1e). For points near the maximum of the co-seismic anomaly below the latitude  $-34^\circ\text{N}$ , a large and sudden jump is observed between February and March 2010, starting from a high value in the time series in February. As we move towards the North (above latitude  $-34^\circ\text{N}$ ), away from the epicenter, the co-seismic jump decreases while an anomalously large positive trend is observed in the preceding months, leading to a slow jump in the time-series. Because of this gradual increase, ending up with two highly anomalous values in January and February 2010, we infer a duration of the signal of at least 2 months. At the monthly resolution of the used GRACE data, and in the presence of hydrological contributions, it remains difficult to point out the exact starting time of this signal, which might be earlier in 2009, and whether it develops continuously or through pulses at submonthly timescales.

We have assessed the sensitivity of the February 2010 GRACE monthly geoid to the co-seismic mass redistributions. The Maule earthquake took place at 6 : 30 UTC on February 27, 2010. When counting the number of February 2010 orbits in a  $20^\circ$  vicinity of the epicenter, we find less than 5% of the monthly orbits in the time interval after the rupture. This confirms that the February 2010 signal North of the epicenter is not significantly impacted by the co-seismic signal, and that the latter which is first recorded in the March 2010 geoid.

## 3.2 Singularity of the gravity gradient signal before the rupture

We have investigated the unique character in space and time of the gravity gradient increase before the earthquake. The spatial unicity over the South American continent is illustrated from Fig. 1a, where the signal near Maule appears as the largest one. The unicity of this signal in time can be directly observed from the time series in Fig. 1e. These time series show that, in the considered region near the Maule 2010 epicentral area, a signal of a comparable amplitude had not been recorded before, nor in the consecutive years (note that the annual cycle correction may degrade in the end of the time series). This is confirmed when repeating the same time series analysis as described above, for hypothetical earthquake times  $t_e$  spanning the [March 2004 - March 2010] interval with a monthly time step. Appendix Fig. S4 shows the obtained anomalous signals cumulated over the  $[t_e - 9 \text{ months to } t_e - 1 \text{ month}]$  intervals: there is no equivalent to the July 2009 - February 2010 gravity gradient signal over the whole period and the whole continent.

## 3.3 Investigation of other GRACE gravity solutions

To assess the robustness of the signals before the rupture, we tested whether they could also be found in two other sets of GRACE geoid models, the CSR06 and the ITSG-2016 solutions, ~~in addition to the GRGS solution~~. For that, we extracted their common space-time patterns of variability using a Singular Value Decomposition between pairs of models (expressed in terms of gravity gradients): 1. GRGS03 versus CSR06 and 2. GRGS03 versus ITSG-2016. We found a highly coupled behaviour of each pair of solutions, featuring a slow jump initiated a few months before the earthquake in the region of the pre- and co-seismic signals, in both the North-South and the East-West directions (~~Appendix Fig. D.2~~) (Appendix D.2, Appendix Fig. S5). As each individual solution, the average of these three datasets shows the same behaviour (Fig. 2a-d). It is illustrated by the following analysis allowing us to identify a slow jump near March 2010 completed to a large extent in February 2010. As the CSR and ITSG-2016 solutions show ~~more a higher level of strip-~~ing noise than the GRGS one, we use a more constrained time evolution model, with less

degrees of freedom than done for GRGS in the previous section. For that, in each set of GRACE solution as well as ~~and~~ in their average, we estimated a Heaviside step function in March 2010. This estimate is not very sensitive to the exact timing of the step, due to the length of the time series: it will not distinguish between steps completed in February or in March. We define anomalous signals in February 2010 such that their amplitude exceeds 50 % of the estimated step, and their probability of occurrence is low (assuming a Gaussian distribution of the monthly gravity gradient values, as done before).

Figure 2 presents the results obtained for each of the three gravity gradient solutions ~~used in this study for one direction (North-South)~~ (in the North-South direction) and for their average ~~for two ranges of orientations (North-South and East-West)~~ (in the North-South and East-West orientations). A good agreement is found between the three solutions: the North-South oriented gravity gradient exhibits an anomalous increase before the earthquake in the same area for each individual solution and their average (Fig. 2a-d). The ~~above-discussed~~ temporal pattern of a slow jump in the gravity gradients is detected in both North-South and East-West directions (Fig. 2f-g). It is associated with a well-resolved spatial pattern in the same area for both orientations, pointing to anomalously large signals during that month (Fig. 2d-e). This behaviour appears unique over all South America (Fig. 2a-c). ~~Finally, we have also~~ We finally investigated anomalously large signals in February 2010 without any constraint on a step-like evolution of the time series. A few other signals are detected in the CSR and ITSG-2016 solutions, in addition to the gravity gradient increase before the Maule earthquake (Appendix Fig. S11). However, the ~~singularity~~ specificity of the February 2010 signal in the region of Maule is further evidenced from comparisons with hydrological models and in-situ data.

## 4 Sources of the gravity signal before the earthquake

### 4.1 Inaccuracies in the GRACE data processing

We have investigated whether the gravity signal before the Maule earthquake could result from inaccuracies in the data analysis: (1) striping artefacts, (2) errors in the atmospheric dealiasing model, or (3) over or under-correction of the seasonal cycle. First, we estimated empirically the level of striping errors in the monthly horizontal gravity gradients from 2003 to 2014, for the 500-1000km spatial scales. For that, we computed each month the rms of the gravity gradients over a wide oceanic area centered at the latitude of the Maule earthquake epicenter. We conclude that the February 2010 anomalous gravity gradient variations exceed the noise by a factor 4 to 8 depending on the spatial scale. Looking then at the atmospheric dealiasing model of the GRGS geoids, based on the ECMWF ERA-Interim reanalysis [10], we find that, in the region of Maule, the amplitude of the February 2010 non-seasonal atmospheric signal is hundred times smaller than the GRACE-observed anomaly before the rupture. This reflects the fact that the modelled atmospheric contribution is almost purely seasonal in the studied area. We finally investigated whether the gravity signal before the earthquake could result from an over- or under-correction of the seasonal cycle in the GRACE data or in the atmospheric model. We first remark that an error in a periodic correction should appear as a periodic residual in the time series. Such behaviour is absent from the gravity gradient time series shown in Fig. 1e until 2011 at least. Comparing the amplitude of the GRACE pre-seismic signal with that of the seasonal cycles fitted in the GRACE data or in the modelled atmospheric contribution at the ~~same~~ ~~location (north of the epicenter)~~ **north of the epicenter**, we notice that the February 2010 ~~anomalous GRACE~~ gravity gradient signal is at least two times larger than the amplitude of the GRACE seasonal cycle and ten times larger than that of the atmospheric model ~~there~~. Thus, neither the striping artefacts nor the atmospheric or seasonal corrections can explain the observed variations.

## 4.2 Hydrological signals from global and regional models

### 4.2.1 Predicted signals in the vicinity of the epicentral area

Most of the gravity signal recorded by GRACE comes from continental water mass redistribution, so we investigated a possible hydrological source to the gravity gradient increase before the earthquake. **Note that the GIA gravity gradient signal from the Patagonian Ice Field does not affect our results due to different timescale, and even more so as we have removed a long-term trend from the data.** The horizontal gravity gradients increase corresponds to mass decrease, hence a drying signal. We first compare the GRACE anomaly with the predictions of the hydrological models presented in the Section 2.2.

In addition to the scale 800-km, we present here the results at the 500-km scale. As shown in Fig. 3, this 500-km scale gives access to finer details including large hydrological signals that might be not resolved at the 800-km scale (Fig. 3c,e). This higher resolution is ~~interesting because it~~ provides a better spatial separation between sources in the Andean Cordillera and those in the watersheds of Argentina, especially the major La Plata basin (hydrological context map Appendix Fig. S7). This smaller spatial scale is closer to the characteristic scale of some drainage basins in the region than the scale 800-km ; at the same time it brings other challenges as we notice a higher number of anomalous signals in the GRACE gravity gradients. They include a large negative anomaly in the La Plata basin (labelled 3 in Fig. 3c), and a positive anomaly around the point ( $294.5^{\circ}\text{E}$  ;  $-31^{\circ}\text{N}$ ), labelled 2 in Fig. 3c. This positive signal is located at the North-East of the 800-km scale GRACE anomaly before the earthquake, which integrates the 500-km scale anomalies 1 and 2 (Fig. 3e).

We first compare the time evolution of the GRACE-observed signal with that predicted from the hydrological models at locations spanning the corresponding area. Fig. 3a shows that GRACE and the models are coherent in the North-Eastern lobe (anomaly 2). In the southern lobe closer to the epicenter (anomaly 1, especially between latitudes  $-33^{\circ}\text{N}$

and  $-34.5^{\circ}\text{N}$ ), GRACE and the models agree from 2004 to the end of 2009 but this consistency degrades starting from January 2010, after five years of low variability. At the beginning of 2010, the GRACE time series indeed exhibit a fast and large increase whereas the hydrological signals remain in the continuity of the previous years. Thus, the North-Eastern component of the GRACE signal (anomaly 2) is probably impacted by a hydrological contribution near the western end of the Plata basin, a temperate climate area (Fig. 3d, Appendix Fig. S8), while the South-Eastern component of the signal (anomaly 1) remains anomalous with respect to the hydrological models. Interestingly, it is located in an arid zone, as discussed later in this work.

#### 4.2.2 Spatial patterns of the modelled hydrological signals

These differences are confirmed when investigating the localization of the hydrological signals. Because the GRACE signal is probably not related to a variation in the seasonal cycle, we investigate the spatial patterns of the residual non-seasonal variability. During the 6 months period before March 2010 (September 2009 - February 2010) as well as in the 7 years before, the GLDAS, WGHM and MGB models do not predict any non-seasonal 500-km scale signal in the region of the GRACE anomaly 1, in both North-South and East-West directions (Appendix Fig. S8, S9). The hydrological signals are indeed controlled by the topographic reliefs of the Andes and the Chilean Coast Range, which localizes the rainfalls in a thin North-South elongated band on the Western flank of the mountains in Southern Chile, mostly south of the considered area. In contrast, the GRACE anomaly 2 is likely affected by a non-seasonal hydrological contribution from the western part of the La Plata basin. When comparing the hydrological models, we found a disagreement of ERA5-Land with the other models. This is mostly due to differences in the seasonal cycle predicted by this model, leading to residual annual signals in the region of Maule (Appendix Fig. S10), unobserved by GRACE.

### 4.2.3 Comparison of different hydrological basins

In a last comparison, we estimated the GRACE anomalous signals in February 2010 in all the investigated gravity field solutions (GRGS, CSR and ITSG-2016) **the GRGS, CSR and ITSG gravity field solutions** without any hypothesis on a step-like evolution of the time series in March 2010. With a lower level of abnormality of the February 2010 signal than in Fig. 1, we detect anomalous gravity gradient variations also over the Orenoco, Chaco and La Plata basins (Appendix Fig. S7, S11). These anomalous ~~gravity gradient~~ variations are probably related to the 2009-2010 El Niño event, which resulted in large mass redistributions associated with droughts in the Amazon basin and floods in the La Plata basin. We notice that the GRACE signals agree well with the predictions of the hydrological models in all the drainage basins, except for the anomaly located north of the epicenter of the Maule earthquake (Appendix Fig. S11). There, El Niño brings increased precipitations in winter (from June to December), and has no direct impact on the summer rainfalls [7]. Thus, it seems hardly consistent with the GRACE mass variations in this area, contrary to the other basins.

## 4.3 In situ observations

As a complement to the hydrological models, we investigated in-situ observations of horizontal and vertical water fluxes (river discharges, precipitations and evapo-transpiration).

The GRACE signal is located in the region of Mendoza in Argentina, considered arid with its 150 to 300 mm of annual rainfall (Fig. 4a), and part of the so-called Arid Diagonal of South America. Most of the water in the watersheds comes from the annual melting of snow and ice and is transported from the mountain by the rivers ; it is collected through artificial dams by the regional population, ~~organized in three oases~~. Therefore, the rivers discharge upstream of the dams is representative of the water influx in the zone and appears significantly correlated with the regional snow accumulation at inter-annual timescales [29]. Fig. 4b-f shows the variations of discharge at five stations upstream of the dams in the



Central Andes over the 2000-2017 period. First, we notice that the annual discharge shows a large decrease starting at the end of 2010. This decrease coincides with the beginning of a mega-drought in Central Chile, manifested as a sequence of dry years with reduced annual precipitations [14]. However, Fig. 4 also shows that the effect of this mega-drought on the river flows is still limited in February 2010; it starts later that year, together with a strong 2010/2011 La Nina episode initiated in June [14]. Thus, this mega-drought cannot explain the GRACE mass decrease signal observed five months before, in February 2010.

Second, we compared the mass anomaly explaining the GRACE signal before the earthquake with the water storage variation corresponding to these discharge data. Here we neglect the impact of the vertical water fluxes, which is consistent with an influx of water mostly from snow and ice melting in this region. The 0.18 mEötvös (resp. 0.19 mEötvös) amplitude of the GRACE signal at the 800-km scale (resp. 500-km scale) can be modelled by a water mass source of width 500-km, length 500-km and thickness 300 mm EWH (Equivalent Water Height). It corresponds to  $\sim 60 \text{ km}^3$  of water storage decrease between the beginning of January 2010 and the end of February 2010, or a discharge of  $30 \text{ km}^3.\text{month}^{-1}$  during two months. Distributing this mass transport over the four major rivers of the region (Mendoza, Desaguadero, Tunuyan and San Juan) still leads to a  $7.5 \text{ km}^3.\text{month}^{-1}$  flow. This is fifteen times more than the largest monthly flow recorded in the region for the period 2000-2017 ( $0.5 \text{ km}^3.\text{month}^{-1}$  for the Mendoza river in 2006, Fig. 4c), and still much larger than the maximum historical discharge of  $1 \text{ km}^3.\text{month}^{-1}$ , recorded in 1987 [32].

To complete our analysis of the hydrological sources in this region, we carried out a more precise estimation of the water storage variations of the four watersheds intersecting the GRACE anomaly, for comparison with the GRACE-observed mass transport in February 2010. For that, we estimate the water storage change (S-S0) at basin scale from in-situ observations of fluxes, namely precipitation grids (P), actual evapotranspiration (E) grids and river specific discharge (Q). These variables are related via the mass balance equation

$\frac{dS}{dt} = P - E - Q$ , which is integrated to derive storage variations per unit surface  $S - S_0 = \int \Delta S dt$ , in mm EWH in each basin, which is transformed in volume in  $\text{km}^3$  by multiplying by the basin area. In the above equation, the river discharge ( $Q$ ) defines the basin response to the effective rainfall ( $P-E$ ). Here, the river discharge stations are located downstream of each basin on which we apply the mass balance equation. As shown in Fig. 5, the obtained water storage variations amount to  $\sim 1.2 \text{ km}^3$  over two months between January and February 2010. This value is far smaller than the dozen of  $\text{km}^3$  of water needed to explain the GRACE signal. Thus, the observed gravity gradient anomaly is not likely to be explained by a water source in this regional context.

## 5 Implications for deep Earth pre-seismic processes

The above analysis supports a solid Earth origin of this gravity gradient signal, involving mass decrease at depth. Here, we discuss its possible origin in the context of the South American subduction.

Multiple lines of evidence indicate that a regional change in stress state inside the crust along the South Chile subduction zone occurred prior to the megathrust earthquake, in relation with deeper slab motions. Bouchon et al [5] report a pre-earthquake seismic activity which began in early January 2010. This activity was characterized by an initial burst of seismic activity at depth followed by shallow foreshocks. In the USGS catalog, a large ( $M_w$  5.8) intermediate-depth earthquake (depth  $\sim 150\text{-km}$ ) occurred on 12 February 2010 in the region where the pre-seismic gravimetric signal is reported, suggesting that the change in stress state affected a very wide area around the epicenter region. Large-scale anomalous GNSS displacements were detected four months before the main event over the whole South Chile subduction zone, corroborating such a hypothesis [2]. The spatial and temporal correlation between the shallow and the deep seismicity activities, the extensional mechanism of the deep shocks and the trenchward motion of 4-8 millimeters lead the authors of these previous studies to the same conclusion. Bouchon et al. [5] and Bedford

et al. [2] propose that these observations are related to a sudden increase of slab pull at depth interacting with shallow slow slip further updip.

All these observations support an extensional deformation of the slab along its subduction direction. Also observed in the case of the 2011 Tohoku-oki earthquake [36], such deformation is consistent with our GRACE pre-seismic mass decrease signal. To evaluate its magnitude, we modeled a pre-seismic intra-slab extension using a model of quasi-static normal faulting in a vertically stratified elastic medium. We found that the observations can be explained by 1.5 m of slip along a  $45^\circ$  dipping, North-South striking plane of width 100-km and length 500-km, located between the depths 115 and 185-km (Fig. 6). This corresponds to a Mw 8.2 event over a few months. As in the case of the Tohoku-oki earthquake, where a precursor signal equivalent to a Mw 8.4 rupture was detected [36], the magnitude of the pre-seismic event is smaller than that of the consecutive co-seismic rupture and its spatial extent is commensurate with the length of the co-seismically ruptured area. This corresponds to a smaller amount of deep deformation distributed over a wider zone around 250-km depth before the Tohoku-oki 2011 earthquake, and a larger but more localized deformation around 150-km depth before the 2010 Maule earthquake.

Interestingly, for both Maule and Tohoku, this pre-seismic gravity signal occurs in a region where the geometry of the subduction changes. The Tohoku pre-seismic signal coincides with a change in the strike of the subduction, in the vicinity of a triple junction. In the case of Maule, the gravity pattern before the rupture is located  $\sim 400$ -km North-East of the epicenter, in a transition section where the dip of the subducted Nazca plate changes sharply. North of  $-33^\circ\text{N}$ , the Nazca plate remains sub-horizontal at about 100-km depth for several hundred kilometers, before dropping steeply into the mantle. South of  $-33^\circ\text{N}$ , the slab plunges continuously at an angle of  $25^\circ$  [6] [38]. This change of dip is associated with a slab hole at  $\sim 200 - 300$ km depth, at the latitudes of the February 2010 GRACE signal [28] [38]; mantle flow through this opening at depth in the flat slab is suggested from seismic tomography. The rapid change of slab geometry causes an increase of the

slab stresses, due to localized lateral deformations[1]. In addition, mantle flow beneath the flat slab and through the slab hole [28] [13] may contribute to entrain the motion of the subducted plate towards the depth.

The spatial and temporal synchronization observed between the pre-seismic gravity signal with the megathrust earthquake suggests that these two events are linked. We thus propose that, between the end of 2009 and March 2010, the deep pre-seismic slab deformation migrated both upwards to the surface and laterally along the slab. From the pre-seismic to the co-seismic phase, the gravity gradient signal indeed shifts from the North/East (around the point  $292^{\circ}\text{E}$ ;  $-32.5^{\circ}\text{N}$ , corresponding to a 150-km depth for the top of the slab) to the South/West (around the point  $290^{\circ}\text{E}$ ;  $-36^{\circ}\text{N}$ ). This lateral migration towards the surface is reminiscent of the variations of coupling of the subduction interface, at the shallower depths. The pre-seismic extension is indeed located down-dip a transition area between a low coupling segment in the North and a high coupling one in the South [31], and the motion propagates towards the more coupled zone in the South, where the rupture occurred [31] in the historical seismic gap of central Chile [48]. Comparing our co-seismic gravity gradient signal with that predicted from a geodesy-based co-seismic slip distribution model [27], we found a reasonable agreement between the GRACE-derived co-seismic anomaly and the modelled one (Appendix Fig. S12).

Finally, the existence of a gravity gradient signal without large surface displacements had been noticed for both the pre- and co-seismic signals of the Tohoku-Oki earthquake, and is again observed in the case of the Maule earthquake. In the Maule pre-seismic phase, the slab deformation estimated above should have generated centimetric surface displacements, which is one order of magnitude greater than the displacements highlighted by Bedford et al.[2]. Even if the spatial coverage of the GNSS network is very sparse in this region far of the trench, it is unlikely that such ground surface displacement remains undetected. Considering other processes that may have contributed to the observed pre-seismic gravity variation, we have investigated the effect of transient fluid release related

556 to oceanic plate dehydration. Upon subduction, hydrous minerals release water from the  
 557 slab over a range of depths [12] [37] [45] [20]; the mechanisms, dimensions and timescales  
 558 of fluid flow within the subduction zone are not well understood. Dehydration fluid is  
 559 generally considered as a continuous process occurring on a time scale of  $10^5 - 10^6$  years  
 560 [12] [20]; however, it has been suggested that channelized fluid flows are highly localized,  
 561 accumulating and releasing high fluid volumes within short time interval (1-4 months) [20]  
 562 [37] [45]. The increasing slab pull force accommodated by extensional cracks and motion  
 563 along normal faults may have promoted the creation of fluid pathways, improving the  
 564 drainage of the subducting plate. Even if the mechanisms of large-scale fluid release from  
 565 the slab at depth remain unclear, a simple model based on a slight change of the porosity  
 566 ( $10^{-5} - 10^{-6}$  of relative volume variation) of the slab segment in extension at depth is able  
 567 to fully or partially explain the the observed gravity gradient signal. We have modelled  
 568 the gravimetric signal caused by a fluid infiltration in the cracks generated by a deep  
 569 extension, i.e. a density variation of  $\rho_{\text{fluids}} - \rho_{\text{rocks}} = -2400\text{kg.m}^3$  over a volume of width  
 570 200-km, length 500-km and thickness 80-km, with a porosity  $\frac{\delta V}{V} = 5 \cdot 10^{-6}$ , located around  
 571 150-km depth. According to this model, the fluid-related mass transfer at depth induced a  
 572 widespread gravity variation (Fig. 6e-f), able to explain the observed gravity gradient signal  
 573 (Fig. 6a-b). We thus hypothesize that the absence of large surface displacements could  
 574 be related to a significant contribution to the observed gravity signal of such deeper mass  
 575 redistributions associated with fluid migration, accompanying the extensional deformation  
 576 of the slab.

## Conclusion

From a dedicated analysis of time series of GRACE-derived gravity gradients, we have detected an anomalously large gravity gradient increase in the months before the Mw 8.8 2010 Maule earthquake, in the north of the epicentral area, most likely caused by mass redistributions at depth within the solid Earth on the continental side of the subduction. This gravity signal prior to the rupture can be explained by a deep extensional deformation of the slab along the subduction direction, equivalent to a Mw 8.2 normal faulting event. This event is commensurate with the precursor signal detected before the Tohoku-Oki earthquake [36], and also located in a region of changes in the geometry of the subducted slab. In the case of 2010 Maule earthquake, the pre-seismic mass decrease signal highlights a larger amount of mass anomaly distributed over a more localized zone with a length commensurate to that of the co-seismically ruptured area. We notice that the modelled Maule pre-seismic normal faulting event should have generated centimetric surface displacements, which have not been observed by GNSS [2]. This leads us to propose that part of this gravity signal could reflect deep mass redistributions from large-scale fluid release promoted by extensional cracks and normal faults in the subducted slab - even if it remains difficult to decipher without ambiguity the physical processes at the origin of the gravity variations observed prior these two earthquakes. Nevertheless, the existence of these interactions between slow mass variations at depth detected by GRACE and interplate seismicity, opens a new field of research to better characterize and understand the dynamics of the seismic cycle at megathrusts. Observing again such interactions for large earthquakes in the future could lead to a paradigm shift in the study of the seismic cycle, which is today essentially based on the distribution of the recurrence times of large earthquakes for the estimation of the seismic hazard.

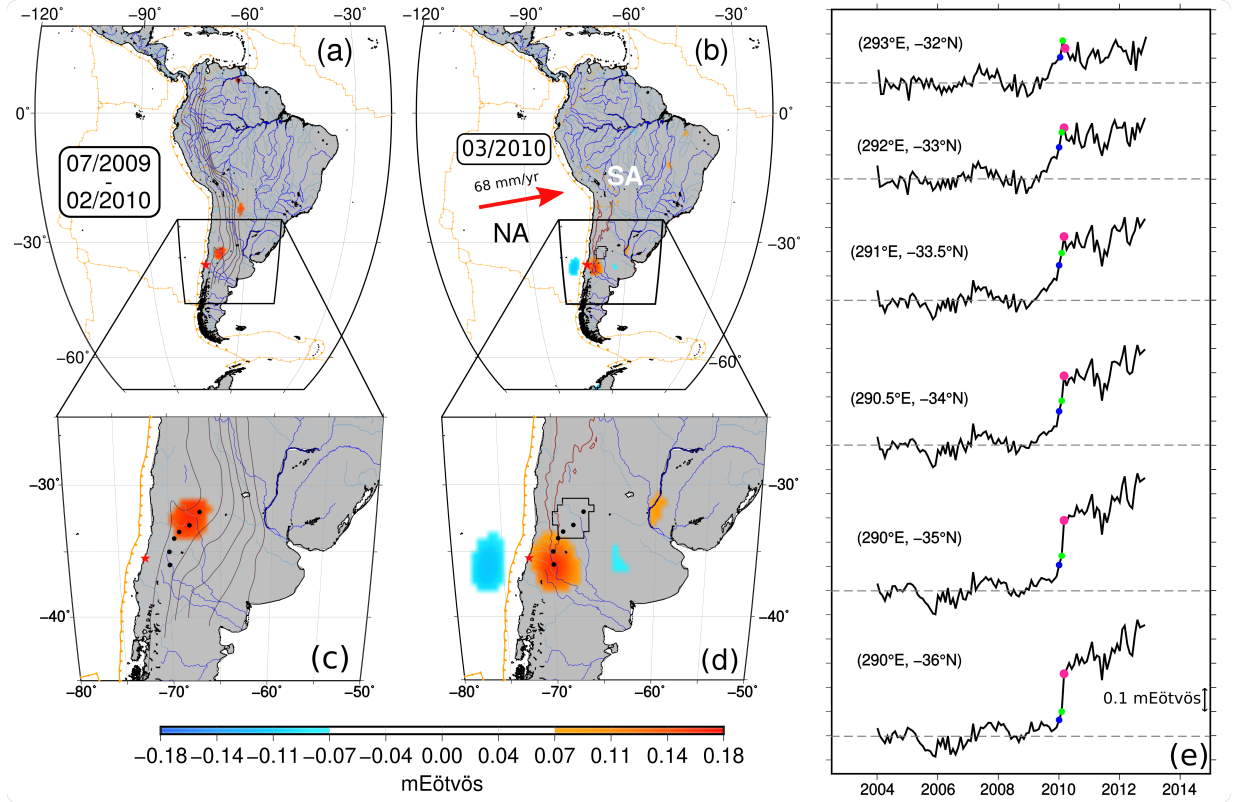


Figure 1: Pre-seismic and co-seismic gravity gradient signals for the Maule earthquake. All panels show the 800-km scale,  $\phi\phi$  GRGS gravity gradients, stacked for  $-10$  to  $10^\circ$  clockwise spherical frame rotations. Panels a and c: cumulated variation over the [July 2009 – February 2010] interval with an absolute amplitude above 0.07 mEötvös, also shown in black contours in the map d. Panels b and d: March 2010 co-seismic variations. Red star: Maule earthquake epicenter; orange lines: plate boundaries [3]; violet lines: Pacific slab isodepth contours every 100-km [16]; brown lines: 3000 m topographic contours. Tectonic plates: NA = Nazca, SA = South-America, Red arrow = subduction direction. Panel e: time series of the gravity gradients after removing the annual and semi-annual cycles and a trend, at locations spanning the pre- and co-seismic anomalies, shown as black dots in the maps c and d. Blue dot in the time series: January 2010 ; green dot: February 2010 ; pink dot: March 2010.

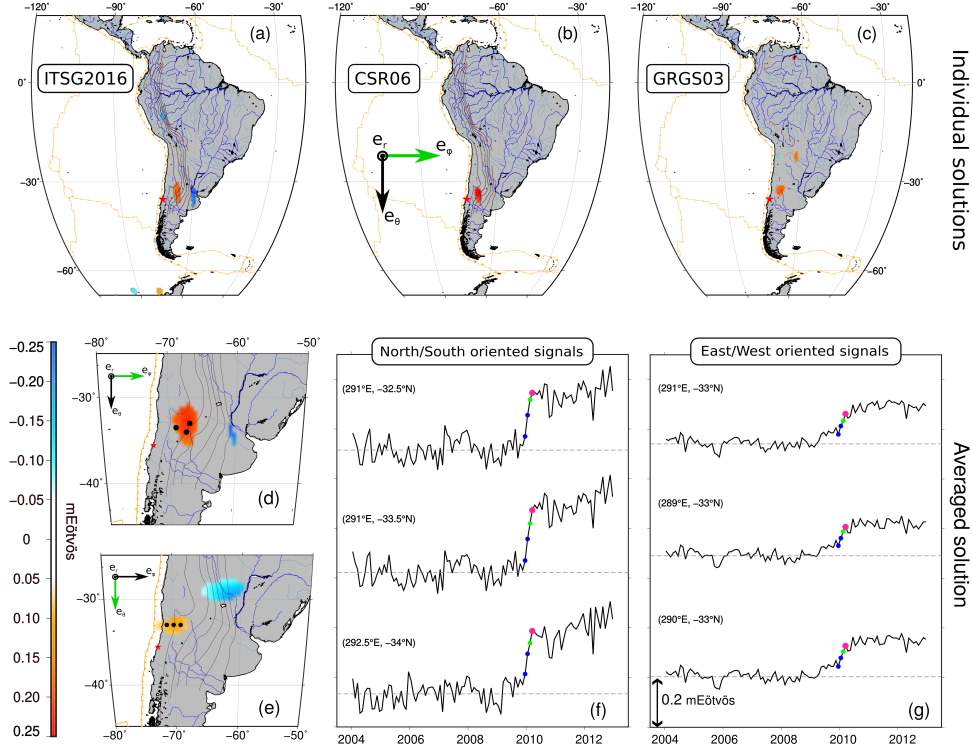


Figure 2: Anomalous gravity gradient signals before the Maule earthquake from the GRGS, CSR and ITSG-2016 gravity solutions and the average of the three solutions. Panels a-d and f : 800-km scale  $\phi\phi$  gravity gradients in the local spherical frame, emphasizing North-South oriented signals. Panels e and g: 800-km scale  $\theta\theta$  gravity gradients in the local spherical frame, emphasizing East-West oriented signals. Top panels: maps for each individual solution. Bottom line panels: maps and time series for the average of the three solutions. Panels a-e: Maps of anomalous gravity gradient signals in February 2010 (with a probability below 0.25% for ITSG-2016, below 1% for CSR, below  $2.5 \cdot 10^{-5}\%$  for GRGS and below 0.01% for the average), persistent in time after March 2010 (see text). Panels f, g: time series of the gravity gradients at locations across the GRACE positive anomaly in February 2010, indicated by the black dots on the maps d, e respectively.



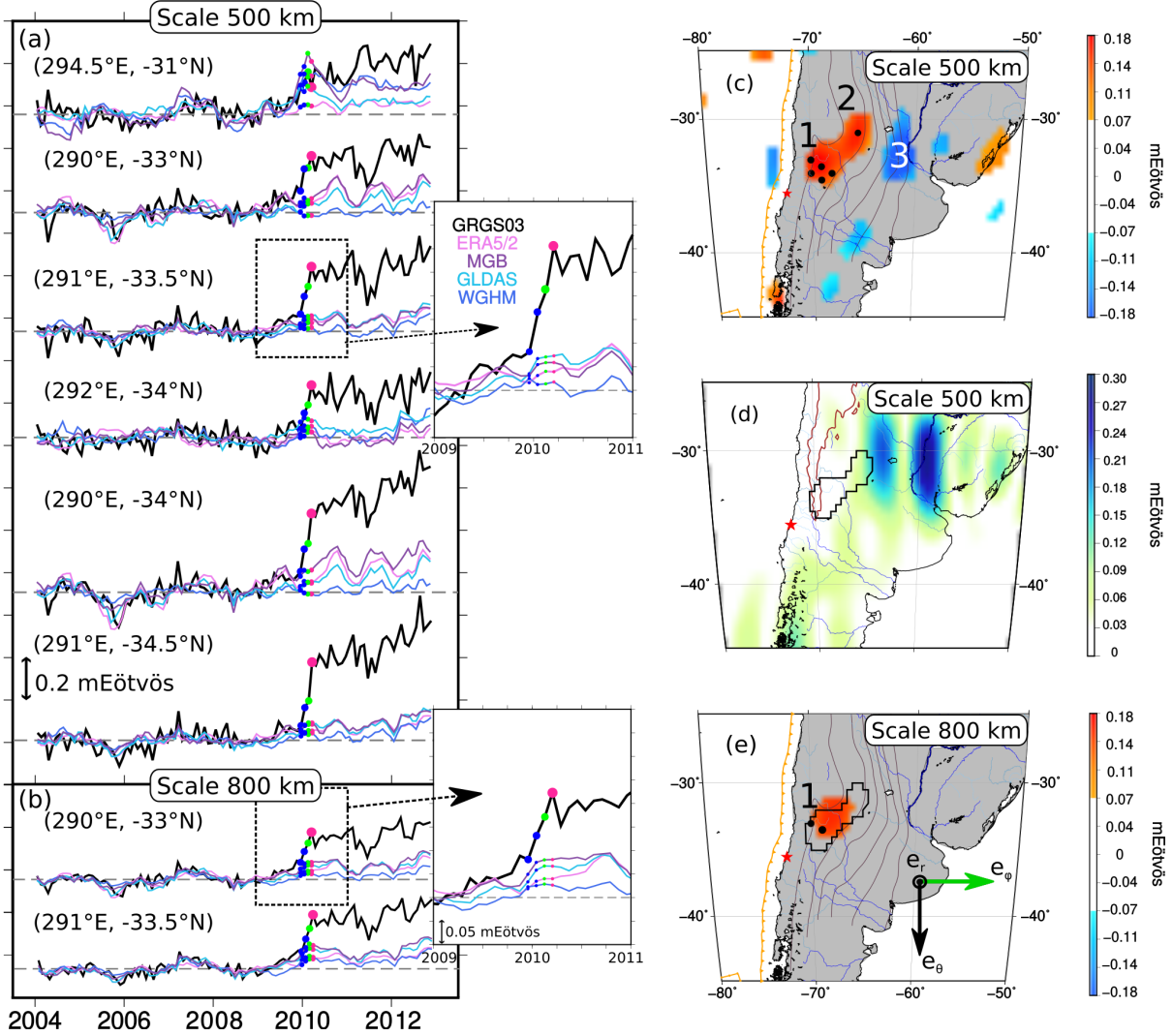


Figure 3: Comparison of the GRACE GRGS gravity gradient signals with those predicted from four hydrological models in the region of Maule at two spatial scales. Panels a,c and d: scale 500-km,  $\phi\phi$  gradients in the local spherical frame. Panels b and e: scale 800-km, same gradients. Panels a (resp. b): time series at points across the GRACE GRGS positive anomaly before the earthquake, marked in black dots in the map c (resp. e). GRGS time series in black ; time series from the hydrological models in colors as referred in the zoomed panel a. The gravity gradients from the ERA5-Land hydrology model have been scaled by a factor 0.5 for consistency with the other hydrological models (Appendix S10). Panels c: Map of the GRACE GRGS anomalous signals before the earthquake. This map is derived from the same analysis as in Fig. 1a, considering a lower level of abnormality of the February 2010 signals (outside the 0.02 - 99.98 percentile range of the long-term distribution). Panel e: same as Fig. 1c. Panel d: Spatial patterns of the non-seasonal signals in the gravity gradients from the WGHM hydrological model, as expressed by the RMS of the 2009/09 – 2010/02 time series after subtraction of the annual, semi-annual and long-term trend components. For panels d and e, black lines are the contours of the positive GRACE GRGS anomaly shown in panel c.

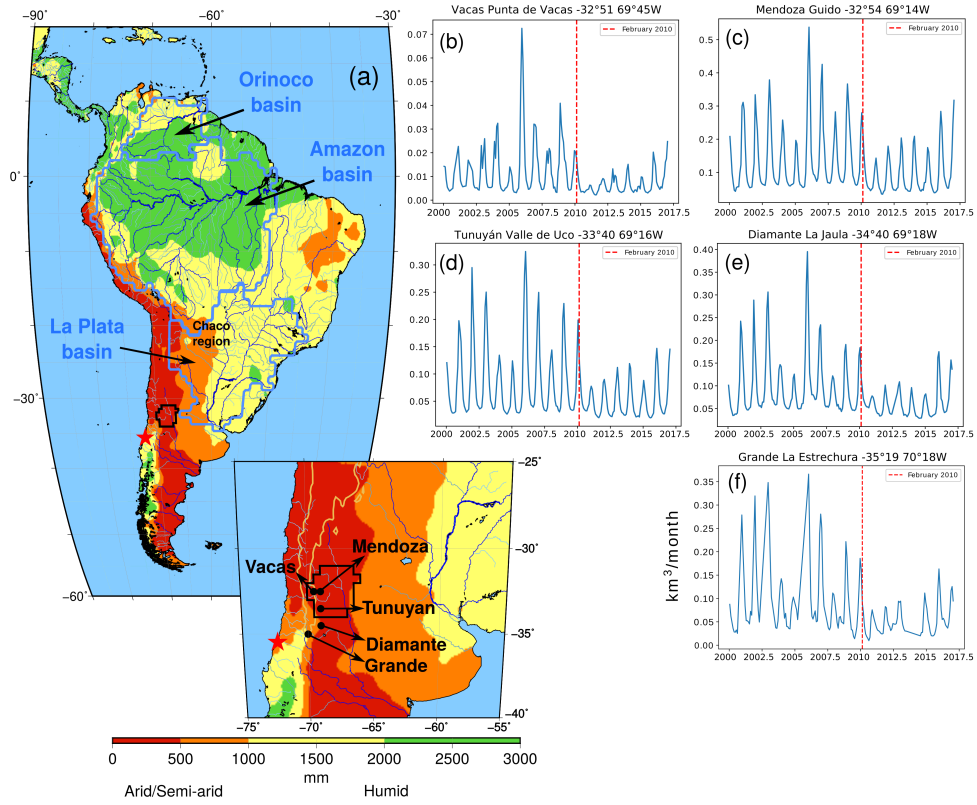


Figure 4: Panel a: map of the different climate zones of South America as reflected by the annual amount of precipitations [23], from arid/semi-arid to humid, superimposed with the contours of the GRACE pre-seismic signal of Fig. 1a (black lines). Panels b-f: monthly river discharge at hydrometric stations in the vicinity of the GRACE pre-seismic signal and upstream of the dams (black dots in the zoomed map of panel a), reflecting the annual supply of water in this arid region by snow and ice melting in the Andean Cordillera. Red dashed line: February 2010.

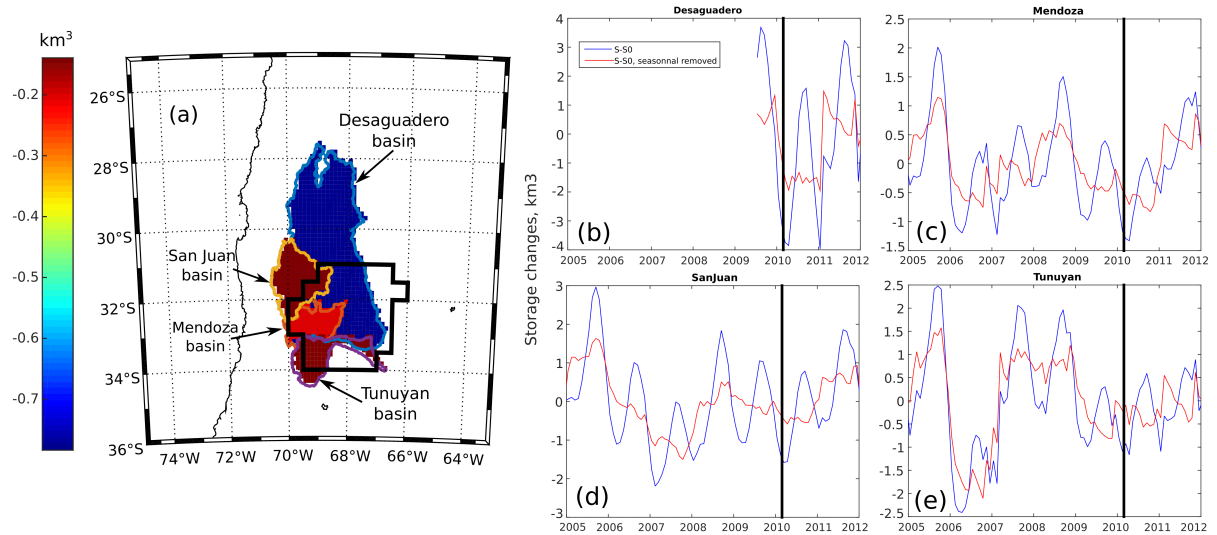


Figure 5: Estimated water storage variations of the Desaguadero, San Juan, Mendoza and Tunuyan basins in the region of Maule. Panel a: mass changes over the basins from the beginning of January to the end of February 2010, superimposed with the contour of the GRACE pre-seismic signal of Fig. 1a (black line). Panels b-e: time series of the water storage variations for each basin, before and after removing a seasonal cycle.

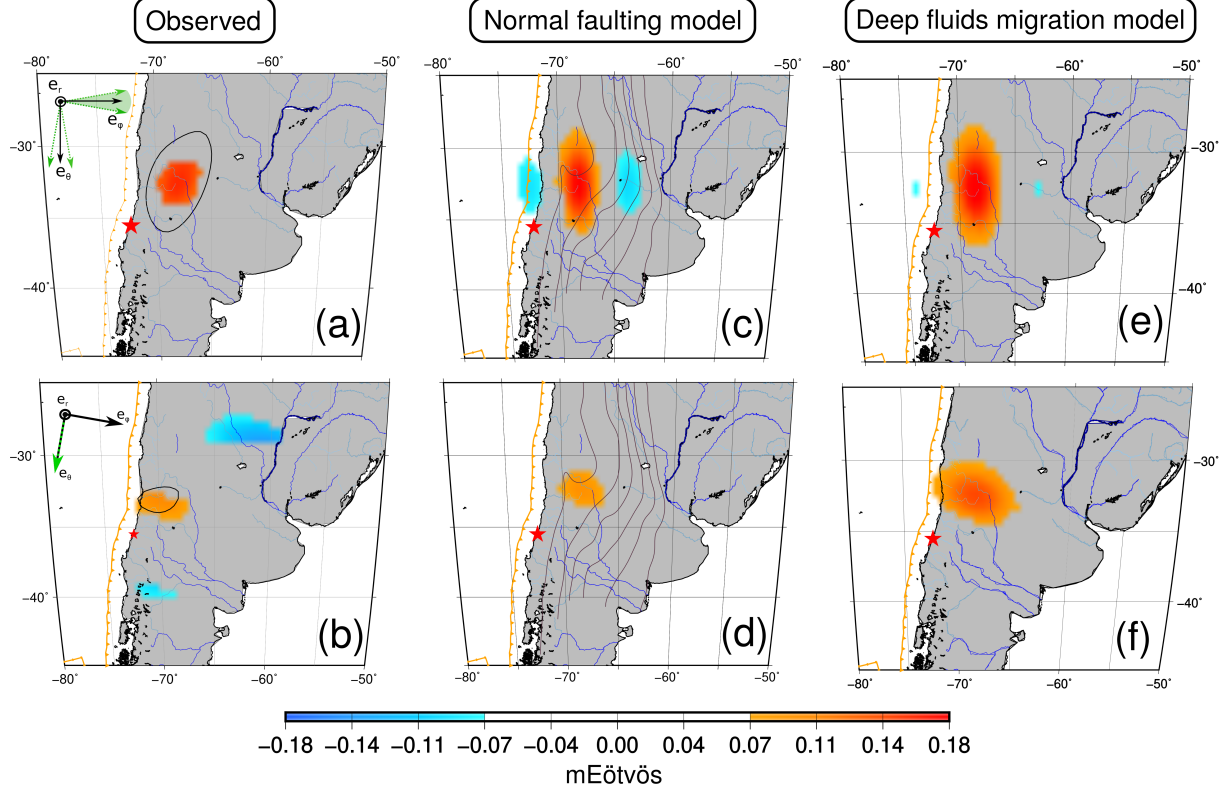


Figure 6: Comparison between the GRGS GRACE-observed (panels a-b) and the modeled (panels c-f) pre-seismic signals for the scale 800-km. Top panels:  $\phi\phi$  gravity gradients, stacked for  $-10$  to  $10^\circ$  clockwise spherical frame rotations ; Bottom panels:  $\theta\theta$  gravity gradients for a  $10^\circ$  clockwise spherical frame rotation. Panel a: same as Fig.1c. The black lines depict the 0.10 mEötvös contours of the February 2010 gravity gradients. Panel b: same as Fig.1c for the considered  $\theta\theta$  gravity gradients. Panels c-d: gravity gradient signals predicted from a model of quasi-static normal faulting in a vertically stratified elastic medium (see text). The violet lines are the slab isodepth contours every 100km [16]. Panels e-f: gravity gradient signals predicted from a model of density variations due to fluid infiltrations over a volume of  $500 \times 500 \times 80$ -km at 150-km depth with porosity  $\frac{\delta V}{V} = 5 \cdot 10^{-6}$  (see text).

## Acknowledgments

This work was supported by CNES. It is based on observations from the GRACE satellites. M.B. was funded by a CNES-IPGP fellowship. We thank Kerstin Schulze, Hannes Müller Schmied and Petra Döll for providing us access to the WGHM hydrology model. We would like to thank Ayan Fleischman, Nicolas Delbart, Emilie Lavie and Jean-Michel Lemoine for their kind support and constructive discussions. Most figures of this paper were generated using the free Generic Mapping Tools software (GMT) [50]. ~~This is IPGP contribution number XXX.~~

## References

- [1] Megan L. Anderson, George Zandt, Enrique Triep, Matthew Fouch, and Susan Beck. Anisotropy and mantle flow in the Chile-Argentina subduction zone from shear wave splitting analysis: CHILE-ARGENTINA SUBDUCTION ZONE. Geophysical Research Letters, 31(23), December 2004.
- [2] Jonathan R. Bedford, Marcos Moreno, Zhiguo Deng, Onno Oncken, Bernd Schurr, Timm John, Juan Carlos Báez, and Michael Bevis. Months-long thousand-kilometre-scale wobbling before great subduction earthquakes. Nature Geoscience, 580:628–635, 2020.
- [3] Peter Bird. An updated digital model of plate boundaries. Geochemistry, Geophysics, Geosystems, 4(3), 2003. eprint: <https://agupubs.onlinelibrary.wiley.com/doi/pdf/10.1029/2001GC000252>.
- [4] Eva Boergens, Elena Rangelova, Michael G. Sideris, and Juergen Kusche. Assessment of the capabilities of the temporal and spatiotemporal ICA method for geophysical signal separation in GRACE data. Journal of Geophysical Research: Solid Earth, 119(5):4429–4447, May 2014.
- [5] Michel Bouchon, David Marsan, Virginie Durand, Michel Campillo, Hugo Perfettini, Raul Madariaga, and Blandine Gardonio. Potential slab deformation and plunge prior to the Tohoku, Iquique and Maule earthquakes. Nature Geoscience, 9(5):380–383, May 2016.
- [6] Thomas Cahill and Bryan L. Isacks. Seismicity and shape of the subducted Nazca Plate. Journal of Geophysical Research, 97(B12):17503, 1992.
- [7] Wenju Cai, Michael J. McPhaden, Alice M. Grimm, Regina R. Rodrigues, Andréa S. Taschetto, René D. Garreaud, Boris Dewitte, Germán Poveda, Yoo-Geun Ham, Agus Santoso, Benjamin Ng, Weston Anderson, Guojian Wang, Tao Geng,

Hyun-Su Jo, José A. Marengo, Lincoln M. Alves, Marisol Osman, Shujun Li, Lixin Wu, Christina Karamperidou, Ken Takahashi, and Carolina Vera. Climate impacts of the El Niño–Southern Oscillation on South America. Nature Reviews Earth & Environment, 1(4):215–231, April 2020.

[8] B. F. Chao and J. R. Liao. Gravity Changes Due to Large Earthquakes Detected in GRACE Satellite Data via Empirical Orthogonal Function Analysis. Journal of Geophysical Research: Solid Earth, 124(3):3024–3035, March 2019.

[9] Chunli Dai, C. K. Shum, Junyi Guo, Kun Shang, Byron Tapley, and Rongjiang Wang. Improved source parameter constraints for five undersea earthquakes from north component of GRACE gravity and gravity gradient change measurements. Earth and Planetary Science Letters, 443:118–128, June 2016.

[10] D. P. Dee, S. M. Uppala, A. J. Simmons, P. Berrisford, P. Poli, S. Kobayashi, U. Andrae, M. A. Balmaseda, G. Balsamo, P. Bauer, P. Bechtold, A. C. M. Beljaars, L. van de Berg, J. Bidlot, N. Bormann, C. Delsol, R. Dragani, M. Fuentes, A. J. Geer, L. Haimberger, S. B. Healy, H. Hersbach, E. V. Hólm, L. Isaksen, P. Kållberg, M. Köhler, M. Matricardi, A. P. McNally, B. M. Monge-Sanz, J.-J. Morcrette, B.-K. Park, C. Peubey, P. de Rosnay, C. Tavolato, J.-N. Thépaut, and F. Vitart. The ERA-Interim reanalysis: configuration and performance of the data assimilation system. Quarterly Journal of the Royal Meteorological Society, 137(656):553–597, April 2011.

[11] Bertrand Delouis, Jean-Mathieu Nocquet, and Martin Vallée. Slip distribution of the february 27, 2010 mw= 8.8 maule earthquake, central chile, from static and high-rate gps, insar, and broadband teleseismic data. Geophysical Research Letters, 37(17), 2010.

[12] Besim Dragovic, Ethan F. Baxter, and Mark J. Caddick. Pulsed dehydration and garnet growth during subduction revealed by zoned garnet geochronology and thermodynamic modeling, Sifnos, Greece. Earth and Planetary Science Letters, 413:111–122, March 2015.

- [13] Caroline M. Eakin, Maureen D. Long, Alissa Scire, Susan L. Beck, Lara S. Wagner, George Zandt, and Hernando Tavera. Internal deformation of the subducted Nazca slab inferred from seismic anisotropy. Nature Geoscience, 9(1):56–59, January 2016. Bandiera\_abtest: a Cg\_type: Nature Research Journals Number: 1 Primary\_atype: Research Publisher: Nature Publishing Group Subject\_term: Geodynamics;Seismology;Tectonics Subject\_term\_id: geodynamics;seismology;tectonics.
- [14] René D. Garreaud, Camila Alvarez-Garretón, Jonathan Barichivich, Juan Pablo Boisier, Duncan Christie, Mauricio Galleguillos, Carlos LeQuesne, James McPhee, and Mauricio Zambrano-Bigiarini. The 2010–2015 megadrought in central Chile: impacts on regional hydroclimate and vegetation. Hydrology and Earth System Sciences, 21(12):6307–6327, December 2017.
- [15] Shin-Chan Han, Jeanne Sauber, and Scott Luthcke. Regional gravity decrease after the 2010 Maule (Chile) earthquake indicates large-scale mass redistribution. Geophysical Research Letters, 37(23), 2010. \_eprint: <https://agupubs.onlinelibrary.wiley.com/doi/pdf/10.1029/2010GL045449>.
- [16] Gavin P. Hayes, Ginevra L. Moore, Daniel E. Portner, Mike Hearne, Hanna Flamme, Maria Furtney, and Gregory M. Smoczyk. Slab2, a comprehensive subduction zone geometry model. Science, 362(6410):58–61, October 2018.
- [17] Kosuke Heki and Koji Matsuo. Coseismic gravity changes of the 2010 earthquake in central Chile from satellite gravimetry: COSEISMIC GRAVITY CHANGES IN CHILE. Geophysical Research Letters, 37(24):n/a–n/a, December 2010.
- [18] Matthias Holschneider, Aude Chambodut, and Mioara Mandea. From global to regional analysis of the magnetic field on the sphere using wavelet frames. Physics of the Earth and Planetary Interiors, 135(2-3):107–124, February 2003.



- [19] Erik R. Ivins and Charles G. Sammis. Transient creep of a composite lower crust: 1. Constitutive theory. Journal of Geophysical Research: Solid Earth, 101(B12):27981–28004, December 1996.
- [20] Timm John, Nikolaus Gussone, Yuri Y Podladchikov, Gray E Bebout, Ralf Dohmen, Ralf Halama, Reiner Klemd, Tomas Magna, and Hans-Michael Seitz. Volcanic arcs fed by rapid pulsed fluid flow through subducting slabs. Nature Geoscience, 5(7):489–492, 2012.
- [21] Martin Jung, Markus Reichstein, Philippe Ciais, Sonia I. Seneviratne, Justin Sheffield, Michael L. Goulden, Gordon Bonan, Alessandro Cescatti, Jiquan Chen, Richard de Jeu, A. Johannes Dolman, Werner Eugster, Dieter Gerten, Damiano Gianelle, Nadine Gobron, Jens Heinke, John Kimball, Beverly E. Law, Leonardo Montagnani, Qiaozhen Mu, Brigitte Mueller, Keith Oleson, Dario Papale, Andrew D. Richardson, Olivier Roupsard, Steve Running, Enrico Tomelleri, Nicolas Viovy, Ulrich Weber, Christopher Williams, Eric Wood, Sönke Zaehle, and Ke Zhang. Recent decline in the global land evapotranspiration trend due to limited moisture supply. Nature, 467(7318):951–954, October 2010.
- [22] T. Lay, C. J. Ammon, H. Kanamori, K. D. Koper, O. Sufri, and A. R. Hutko. Teleseismic inversion for rupture process of the 27 February 2010 Chile (Mw 8.8) earthquake. Geophysical Research Letters, 37(13), 2010. \_eprint: <https://agupubs.onlinelibrary.wiley.com/doi/pdf/10.1029/2010GL043379>.
- [23] David R. Legates and Cort J. Willmott. Mean seasonal and spatial variability in gauge-corrected, global precipitation. International Journal of Climatology, 10(2):111–127, 1990. \_eprint: <https://rmets.onlinelibrary.wiley.com/doi/pdf/10.1002/joc.3370100202>.
- [24] Jean-Michel Lemoine, Sean Bruinsma, Sylvain Loyer, Richard Biancale, Jean-Charles Marty, Felix Perosanz, and Georges Balmino. Temporal gravity field models inferred from GRACE data. Advances in Space Research, 39(10):1620–1629, January 2007.

- [25] Yu-nung Nina Lin, Anthony Sladen, Francisco Ortega-Culaciati, Mark Simons, Jean-Philippe Avouac, Eric J. Fielding, Benjamin A. Brooks, Michael Bevis, Jeff Genrich, Andreas Rietbrock, Christophe Vigny, Robert Smalley, and Anne Socquet. Coseismic and postseismic slip associated with the 2010 Maule Earthquake, Chile: Characterizing the Arauco Peninsula barrier effect: CHARACTERIZING ARAUCO BARRIER EFFECT. Journal of Geophysical Research: Solid Earth, 118(6):3142–3159, June 2013.
- [26] Di Long, Laurent Longuevergne, and Bridget R. Scanlon. Uncertainty in evapotranspiration from land surface modeling, remote sensing, and GRACE satellites. Water Resources Research, 50(2):1131–1151, 2014. \_eprint: <https://onlinelibrary.wiley.com/doi/pdf/10.1002/2013WR014581>.
- [27] S. Lorito, F. Romano, S. Atzori, X. Tong, A. Avallone, J. McCloskey, M. Cocco, E. Boschi, and A. Piatanesi. Limited overlap between the seismic gap and coseismic slip of the great 2010 Chile earthquake. Nature Geoscience, 4(3):173–177, March 2011.
- [28] Colton Lynner, Megan L. Anderson, Daniel E. Portner, Susan L. Beck, and Hersh Gilbert. Mantle flow through a tear in the Nazca slab inferred from shear wave splitting. Geophysical Research Letters, 44(13):6735–6742, July 2017.
- [29] Mariano H. Masiokas, Ricardo Villalba, Brian H. Luckman, Carlos Le Quesne, and Juan Carlos Aravena. Snowpack Variations in the Central Andes of Argentina and Chile, 1951–2005: Large-Scale Atmospheric Influences and Implications for Water Resources in the Region. Journal of Climate, 19(24):6334–6352, December 2006.
- [30] Torsten Mayer-Gürr, Saniya Behzadpour, Matthias Ellmer, Beate Klinger, Andreas Kvas, and Norbert Zehentner. ITSG-Grace2016 - Monthly and Daily Gravity Field Solutions from GRACE. 2016.

- [31] Marianne Metois, C Vigny, and A Socquet. Interseismic coupling, megathrust earthquakes and seismic swarms along the Chilean subduction zone (38–18 s). Pure and Applied Geophysics, 173(5):1431–1449, 2016.
- [32] Stella M. Moreiras. Climatic effect of ENSO associated with landslide occurrence in the Central Andes, Mendoza Province, Argentina. Landslides, 2(1):53–59, April 2005.
- [33] Marcos Moreno, Matthias Rosenau, and Onno Oncken. 2010 Maule earthquake slip correlates with pre-seismic locking of Andean subduction zone. Nature, 467(7312):198–202, September 2010.
- [34] Hannes Müller Schmied, Denise Cáceres, Stephanie Eisner, Martina Flörke, Claudia Herbert, Christoph Niemann, Thedini Asali Peiris, Eklavya Popat, Felix Theodor Portmann, Robert Reinecke, et al. The global water resources and use model watergap v2. 2d: model description and evaluation. Geoscientific Model Development, 14(2):1037–1079, 2021.
- [35] Isabelle Panet. An Analysis of Gravitational Gradients in Rotated Frames and Their Relation to Oriented Mass Sources. Journal of Geophysical Research: Solid Earth, 123(12):11,062–11,090, December 2018.
- [36] Isabelle Panet, Sylvain Bonvalot, Clément Narteau, Dominique Remy, and Jean-Michel Lemoine. Migrating pattern of deformation prior to the Tohoku-Oki earthquake revealed by GRACE data. Nature Geoscience, 11(5):367–373, May 2018.
- [37] Oliver Plümper, Timm John, Yuri Y Podladchikov, Johannes C Vrijmoed, and Marco Scambelluri. Fluid escape from subduction zones controlled by channel-forming reactive porosity. Nature Geoscience, 10(2):150–156, 2017.
- [38] Daniel Evan Portner, Susan Beck, George Zandt, and Alissa Scire. The nature of sub-slab slow velocity anomalies beneath South America. Geophysical Research Letters, 44(10):4747–4755, May 2017.

- [39] M. Rodell, P. R. Houser, U. Jambor, J. Gottschalck, K. Mitchell, C.-J. Meng, K. Arsenault, B. Cosgrove, J. Radakovich, M. Bosilovich, J. K. Entin, J. P. Walker, D. Lohmann, and D. Toll. The Global Land Data Assimilation System. Bulletin of the American Meteorological Society, 85(3):381–394, March 2004.
- [40] Bruno Rudolf. The Global Precipitation Climatology Centre (GPCC). page 17.
- [41] S. Ruiz and R. Madariaga. Historical and recent large megathrust earthquakes in Chile. Tectonophysics, 733:37–56, May 2018.
- [42] Himanshu Save, Byron Tapley, and Srinivas Bettadpur. GRACE RL06 reprocessing and results from CSR. page 10697, April 2018. Conference Name: EGU General Assembly Conference Abstracts.
- [43] U Schneider, A Becker, P Finger, E Rustemeier, and M Ziese. Gpcc full data monthly product version 2020 at 0.25°: monthly land-surface precipitation from rain-gauges built on gts-based and historical data. Global Precipitation Climatology Centre at Deutscher Wetterdienst: Offenbach, Germany, 2020.
- [44] Vinícius A. Siqueira, Rodrigo C. D. Paiva, Ayan S. Fleischmann, Fernando M. Fan, Anderson L. Ruhoff, Paulo R. M. Pontes, Adrien Paris, Stéphane Calmant, and Walter Collischonn. Toward continental hydrologic–hydrodynamic modeling in South America. Hydrology and Earth System Sciences, 22(9):4815–4842, September 2018.
- [45] Stephan Taetz, Timm John, Michael Bröcker, Carl Spandler, and Andreas Stracke. Fast intraslab fluid-flow events linked to pulses of high pore fluid pressure at the subducted plate interface. Earth and Planetary Science Letters, 482:33–43, 2018.
- [46] Yusaku Tanaka and Kosuke Heki. Long- and short-term postseismic gravity changes of megathrust earthquakes from satellite gravimetry. Geophysical Research Letters, 41(15):5451–5456, 2014. \_eprint: <https://agupubs.onlinelibrary.wiley.com/doi/pdf/10.1002/2014GL060559>.

- 786 [47] B. D. Tapley. GRACE Measurements of Mass Variability in the Earth System. Science,  
787 305(5683):503–505, July 2004.
- 788 [48] A. Udias, R. Madariaga, E. Bufo, D. Munoz, and M. Ros. The Large Chilean  
789 Historical Earthquakes of 1647, 1657, 1730, and 1751 from Contemporary Documents.  
790 Bulletin of the Seismological Society of America, 102(4):1639–1653, August 2012.
- 791 [49] Lei Wang, C. K. Shum, Frederik J. Simons, Andrés Tassara, Kamil Erkan, Christopher  
792 Jekeli, Alexander Braun, Chungyen Kuo, Hyongki Lee, and Dah-Ning Yuan. Coseismic  
793 slip of the 2010 Mw 8.8 Great Maule, Chile, earthquake quantified by the inversion  
794 of GRACE observations. Earth and Planetary Science Letters, 335-336:167–179, June  
795 2012.
- 796 [50] Paul Wessel and Walter HF Smith. New version of the generic mapping tools. Eos,  
797 Transactions American Geophysical Union, 76(33):329–329, 1995.

## Appendix

### A Gravity gradients at different spatial scales

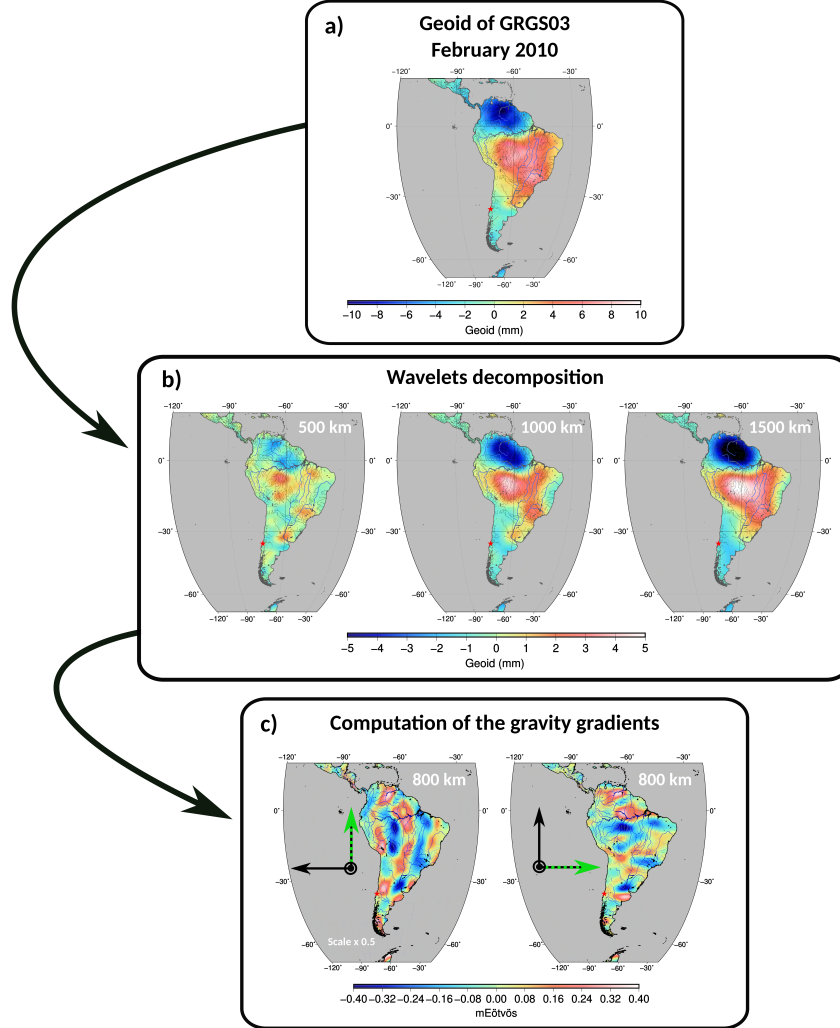


Figure S1: From the geoid to the multi-scale gravity gradients. Panel a: February 2010 geoid map (GRGS gravity solution). Panel b: wavelet analysis of the geoid map shown in Panel a, at different spatial scales (500, 1000 and 1500-km). Panel c: second-order gradients of the 800-km scale wavelet-filtered geopotential. In the spherical approximation, the geopotential is proportional to the geoid. Left (resp. right) panel:  $\phi\phi$  (resp.  $\theta\theta$ ) gravity gradients in the local south-east-up spherical frame.

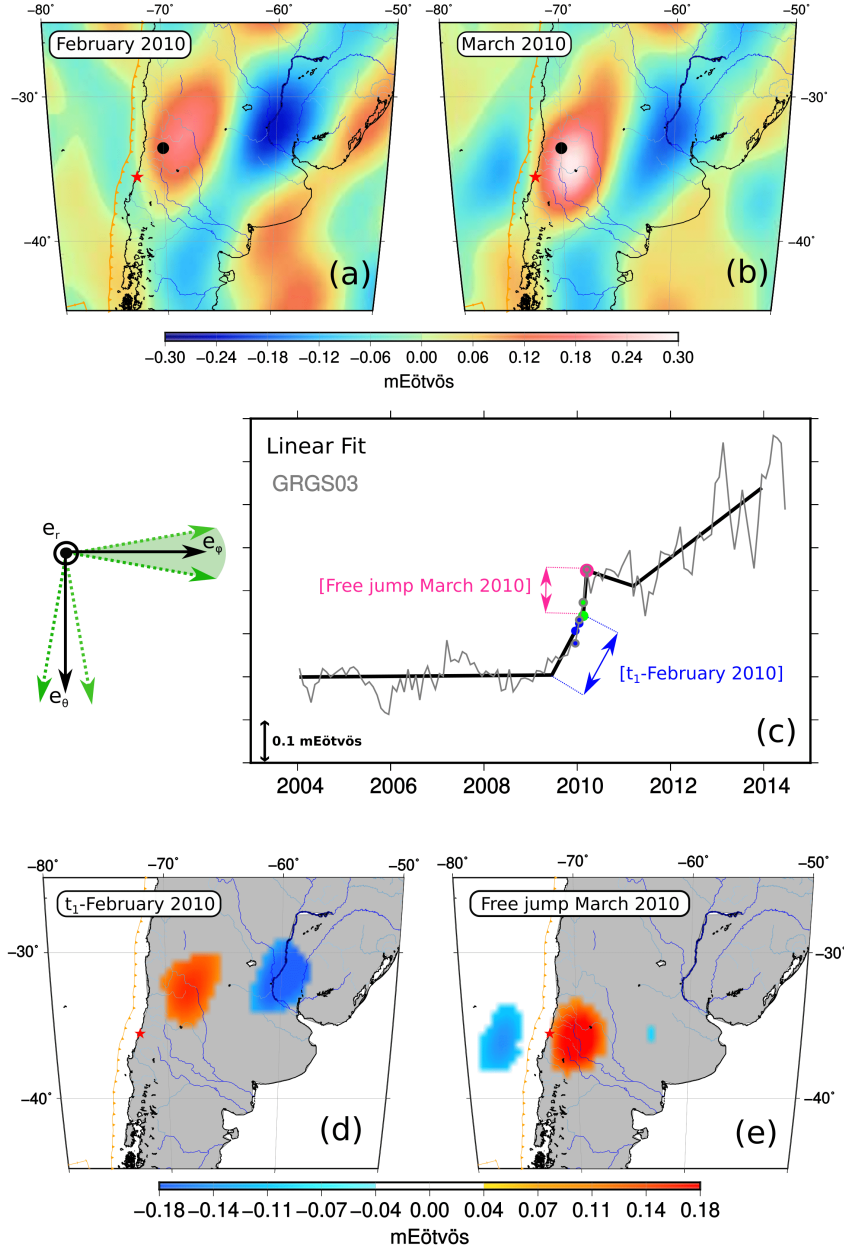


Figure S2: Piece-wise linear fit of the time series of the GRGS gravity gradients (800-km scale,  $\phi\phi$  gravity gradients in the local south-east-up spherical frame, averaged for  $-10^\circ$  to  $10^\circ$  clockwise frame rotations around the radial axis). Panel a-b: maps of the monthly gravity gradients in February and March 2010. Panel c: time series at the location marked by a black dot in the Panels a-b (thin grey line) and their piece-wise linear model (thick black line). Panel d: cumulated variation over the [July 2009 - February 2010] interval, associated with abnormally large signals in February 2010 (probability below  $2.5 \cdot 10^{-4}\%$ ) with an amplitude threshold of 0.1 mEötvös on the eight months trend. Panel e: March 2010 co-seismic signal, associated with abnormally large signals in March 2010 (probability below  $2.5 \cdot 10^{-4}\%$ ). Here, the level of abnormality of the February and March 2010 signals is lower than in Main Fig. 1.

## B Wavelet filtering of the geoid

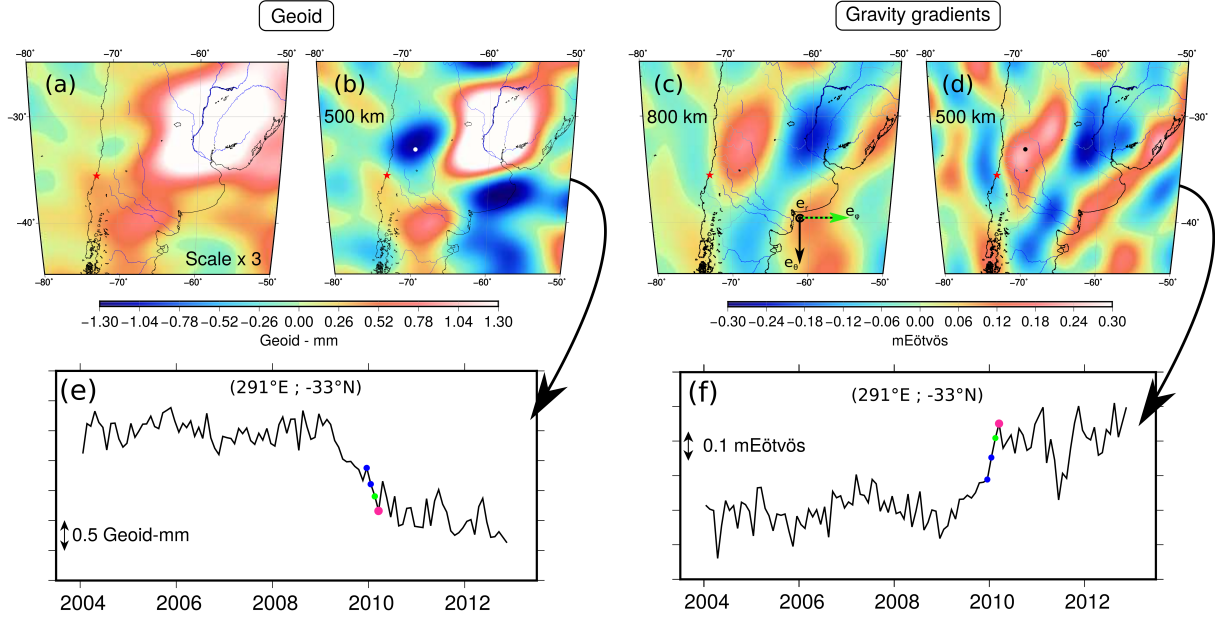


Figure S3: Comparison between the total geoid, the wavelet-filtered geoid and the multi-scale gravity gradients in February 2010 (GRGS gravity solution). Panel a: February 2010 geoid anomaly map. Panel b: 500-km scale wavelet analysis of the geoid, using the same wavelets as for the computation of the multi-scale gravity gradients. Panels c (resp. d): 500-km scale (resp. 800-km scale)  $\phi\phi$  gravity gradients in the local South-East-Up spherical frame, emphasizing North-South oriented signals in February 2010. Panel e (resp. f): time series at the location indicated by the white (resp. black) dot on the maps b (resp. d).

Fig. S3 compares the February 2010 signals in the studied region, as obtained from the total geoid, from the wavelet-filtered geoid and from the horizontal  $\phi\phi$  gravity gradients. The contribution of the major hydrological sources from the La Plata basin predominates in the total geoid (Fig. S3a), partially masking the Maule pre-seismic signal. This smaller signal is emphasized in a high-resolution wavelet filtering of the geoid (Fig. S3b) and can be detected in the corresponding time series (Fig. S3e). However, it is not well separated from the nearby La Plata anomaly, which still perturbs the amplitude of the 500-km scale geoid signal in the region of the pre-seismic anomaly. The horizontal gravity gradients perform a better separation of these two signals, as shown by the comparison of the panel b with the panels c and d, where the amplitude of the La Plata anomaly has considerably



811 decreased and that of the Maule pre-seismic signal starts to predominate. Indeed, the La  
812 Plata signal has a strong East-West component, which is filtered out in the North-South  
813 oriented gravity gradients.

## 814 C Temporal unicity of the GRGS pre-seismic signal

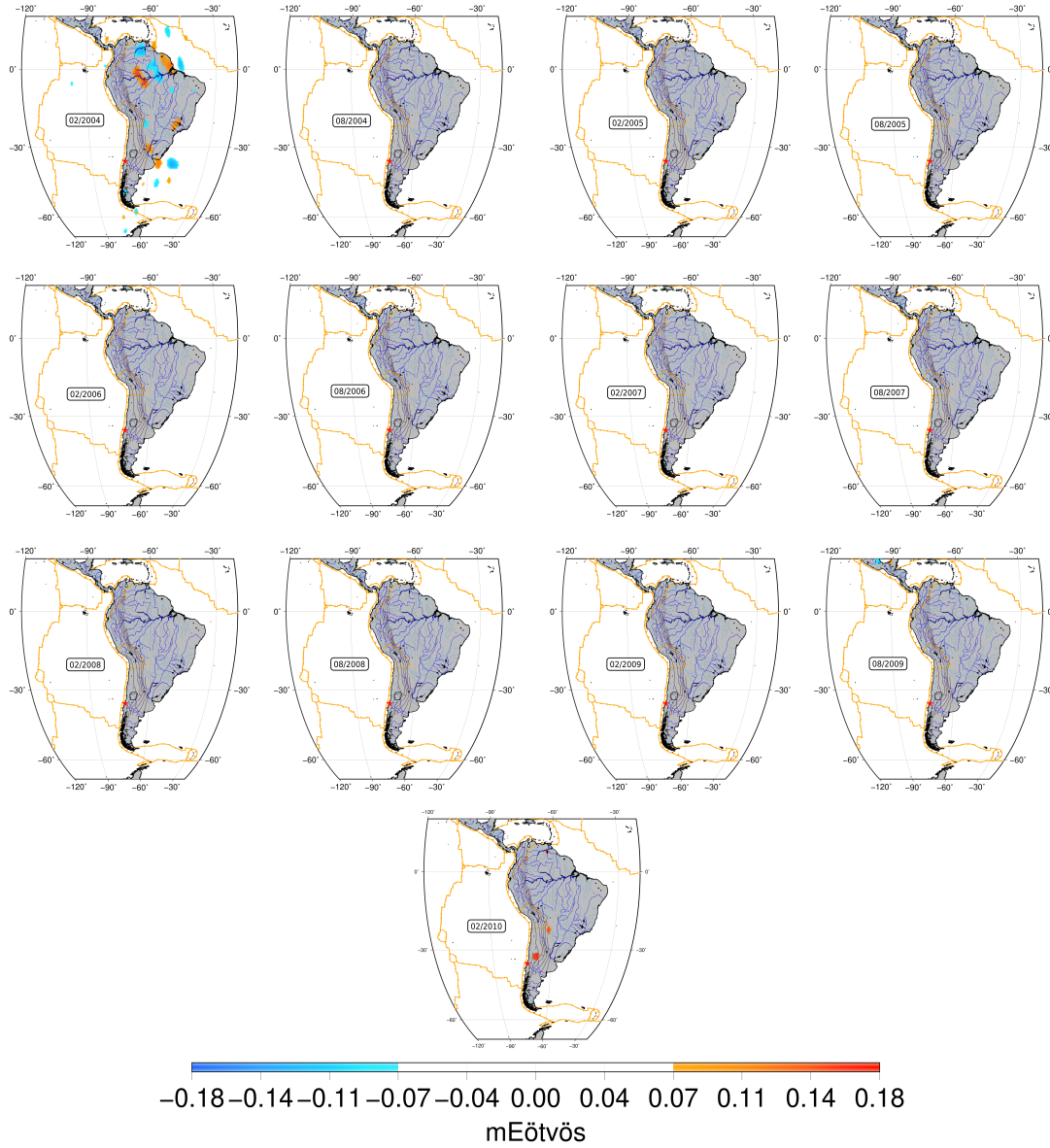


Figure S4: Time series of anomalous gravity gradient signals over South America obtained by applying the same analysis as in Fig. 1a, for hypothetical earthquake times  $t_e$  spanning the [January 2003 – March 2010] time interval. Same scale and orientations of the spherical frame as in Fig. 1.

## D Investigation of other GRACE solutions

### D.1 Signal in individual solutions

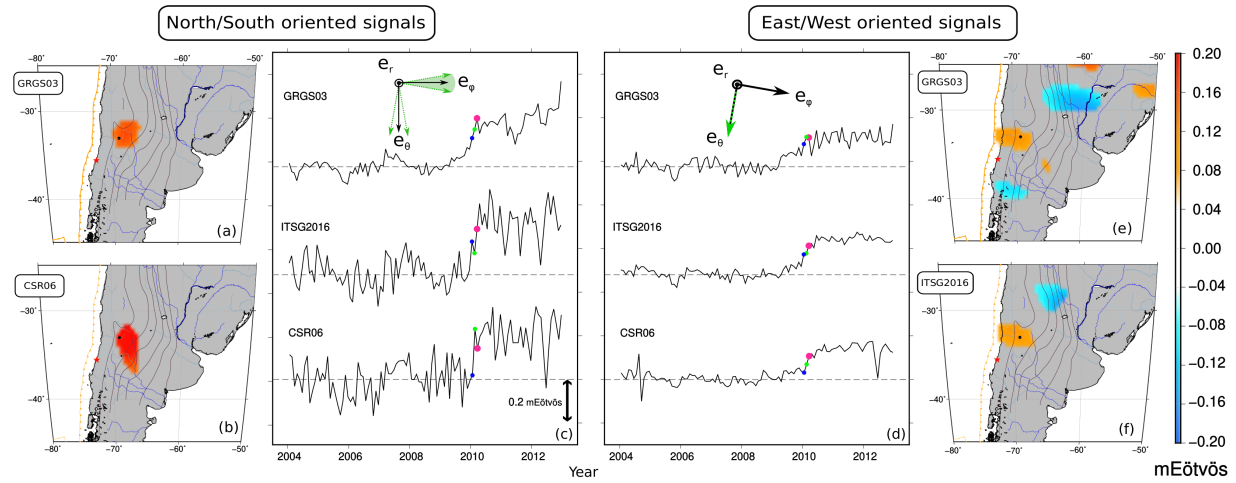


Figure S5: Comparison of the gravity gradient signals before the Maule earthquake from three different gravity field solutions: GRGS, CSR and ITSG-2016. Panels a-c (resp. panels d-f): 800-km scale  $\phi\phi$  (resp.  $\theta\theta$ ) gravity gradients in the local south-east-up spherical frame, emphasizing North-South (resp. East-West) oriented signals. The time series at the point ( $-33^\circ\text{N}$  ;  $291^\circ\text{E}$ ) marked by a black dot on all maps, are compared in panels c-d for each gravity solution and each orientation. Maps a-b compare the spatial patterns of pre-seismic gravity gradient anomalies in the GRGS and the CSR solutions, for the North-South orientation. Maps e-f show the same comparison for the East-West orientation, between the GRGS and the ITSG-2016 solutions. For the GRGS solutions, the spatial signals in the maps a,e are obtained in the same way as in Fig. 1a. For the CSR and ITSG-2016 solutions, the maps represent abnormally large values in February 2010, outside of the [1-99%] (CSR) and the [2.5-97.5%] (ITSG-2016) percentiles of the long-term distributions of the time series, persistent in time after March 2010 (see Main Text, section 3.3).

## D.2 Singular Value Decomposition of coupled fields

### D.2.1 Principle

To identify common spatio-temporal patterns between the three gravity models (GRGS, ITSG and CSR) taken two-by-two, we used a singular value decomposition (SVD). This method is well-suited to identify the coupled space-time patterns of variability between two fields. It is based on the decomposition of the cross-covariance matrix of the two space-time data matrices into a linear combination of orthogonal modes, each expressed by the multiplication of a spatial pattern with a time series. In more detail, the principle is as follows. We first construct the temporal cross-covariance matrix ( $C$ ) between two data fields e.g. GRGS ( $G$ ) and ITSG ( $I$ ). Each data field is represented by a rectangular  $n \times p$  matrix, where  $n$  is the number of epochs and  $p$  the number of locations (grid points in the case of a regular grid), such that  $G_{ij} = g_{\text{GRGS}}(t_i, r_j)$  for the GRGS03 solution,  $I_{ij} = g_{\text{ITSG}}(t_i, r_j)$  for the ITSG solution. Here,  $t_i$  denotes the  $i$ -th epoch,  $r_j$  the  $j$ -th position on the spatial grid,  $g_{\text{GRGS}}$  (resp.  $g_{\text{ITSG}}$ ) denotes the GRGS (resp. ITSG) gravity gradients. We have:

$$C = \text{cov}(G, I) = G^t I \quad (1)$$

Then, we compute the SVD of the cross-covariance matrix  $C$  by solving the following equation, which can be seen as a generalization to rectangular matrices of the diagonalization of the square symmetric matrix:

$$C = ULV^t. \quad (2)$$

We obtain two sets of spatially orthogonal singular vectors (the columns of  $U$  and  $V$  for matrices  $G$  and  $I$  respectively). The diagonal matrix  $L$  contains the singular values associated with each pair of singular vectors. Each common mode is represented by the product between a temporal mode  $a(t)$  and its associated spatial mode  $b(r)$ . The  $i$ -th temporal mode is given by the  $i$ -th column of the matrix  $A = GU$  (resp.  $B = IV$ ) for the GRGS data field (resp. the ITSG data field). The associated spatial patterns are given by the  $i$ -th columns of  $U$  and  $V$  respectively. Finally, the importance of each common mode

is reflected by the fraction of the squared covariance explained by this mode ( $SCF_k$ ). For the  $k^{\text{th}}$  common mode, it is given by:  $SCF_k = \frac{L(k,k)}{\text{trace}(L)}$ .

## D.2.2 Results

In the North-South direction, the first common modes between GRGS and CSR, and between GRGS and ITSG-2016, represent more than 75 % of the squared covariance between each pair of solutions, in both cases (Fig. S6c,k). Thus, they point to a highly coupled behaviour of each pair of solutions. The associated spatial pattern covers the locations of the co-seismic and pre-seismic signals (Fig. S6a,b,i,j); the temporal pattern shows a progressive increase in the gravity gradients over three months up to March 2010, in each gravity gradient solution (Fig. S6d,l). In the East-West direction, the first common modes explain a smaller amount of variance, at the level of 50 % of covariance (Fig. S6g,o) - which is still relatively high. This is due to a larger contribution of the hydrological signals in the La Plata basin in this direction, in the  $2^{\text{nd}}$  mode. The spatial and temporal patterns of this mode are consistent with those obtained in the North-South direction: the spatial pattern is localized in the epicentral region (Fig. S6e,f,m,n), and the temporal evolution shows a progressive step-like variation initiated months before the rupture, stabilized in March 2010 (Fig. S6h,p).

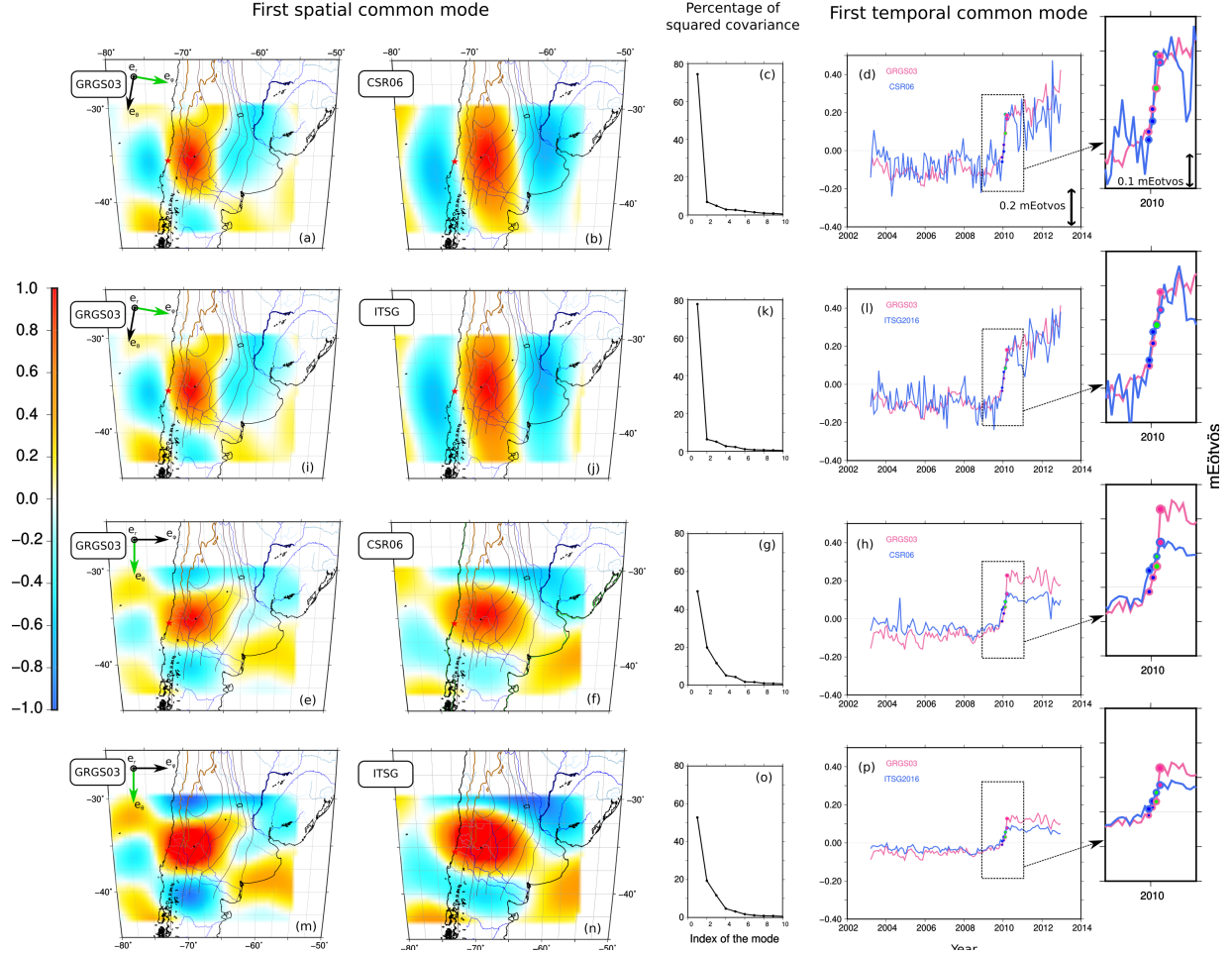


Figure S6: Common modes of variability in the region of Maule between the 800-km scale GRGS gravity gradients and the 800-km scale CSR (top and lower middle lines) or ITSG-2016 (upper middle and bottom lines) gravity gradients respectively, in the North-South direction ( $\phi\phi$  gradients in the local spherical frame, top two lines) and in the East-West direction ( $\theta\theta$  gradients in the local spherical frame, bottom two lines). Columns 1 and 2: non-dimensionalized spatial pattern of the first common mode for each gravity gradient solution ; column 3: percentage of covariance explained ; column 4: dimensionalized time series of the first common mode for each gravity gradient solution. Blue dot in the time series: January 2010 ; green dot: February 2010 ; pink dot: March 2010.

## E Hydrological models and in-situ data

To separate solid Earth and hydrological signals, we designed both a model-driven and a data-driven approach to define the impact of water redistribution on gravity. We considered four complementary hydrological models: 1. The global GLDAS NOAH 2.1 model (including soil moisture, snow and water stored in the canopy) at  $0.25^\circ$  resolution [39], 2. the global WGHM model (including soil moisture, snow, groundwater and surface water) at  $0.5^\circ$  resolution [34], 3. the global ERA5-Land model at 9-km resolution (including soil moisture and snow) [10] and 4. the regional MGB model for South America (including canopy, soil moisture, ground water and surface water) at 10-km resolution [44]. We reconstructed each month the geoid and the gravity gradients predicted by these different models, considering the direct newtonian attraction of the water loads and applying a thin layer approximation. Here, the model ensemble is used to better quantify errors arising from forcing data, model structure, and model spatial resolution. Then, we use the gravity gradient signals predicted from these models for comparisons with the observed ones, in order to discuss the origin of the GRACE anomalies. Comparing these four different models also allow us to identify robust features and model-dependent errors arising from forcing data, model structure, and model spatial resolution.

In specific regions, we complete the model analysis with water storage changes inferred from in-situ observations. We considered observations of river discharge ( $Q$ ), precipitation ( $P$ ) and actual evapotranspiration ( $E$ ). The precipitation is based on the Global Precipitation Climatology Center (GPCC) “Full Data Monthly Version 2020” dataset [43]. The GPCC provides gridded gauge-analysis products derived from quality controlled station data, at  $0.25^\circ$  resolution [40]. The actual evapotranspiration is provided by the Max Planck Institute [21]. It is estimated from a data-driven approach, based on a global monitoring network, meteorological and remote-sensing observations, and a machine-learning algorithm. Finally, we used river discharge data and basin outlines provided by the Global Runoff Data Centre (GRDC). The hydrological analysis is performed over 2005-2012 when

888 discharge data is available, in order to remove properly ~~an~~ annual and semi-annual signals.  
889 Furthermore, in order to remove the potential impact of systematic bias in the fluxes data  
890 (e.g. [26]), a linear trend is fitted on water storage changes over the 2005-2012 period.

891



892 F Hydrological context map

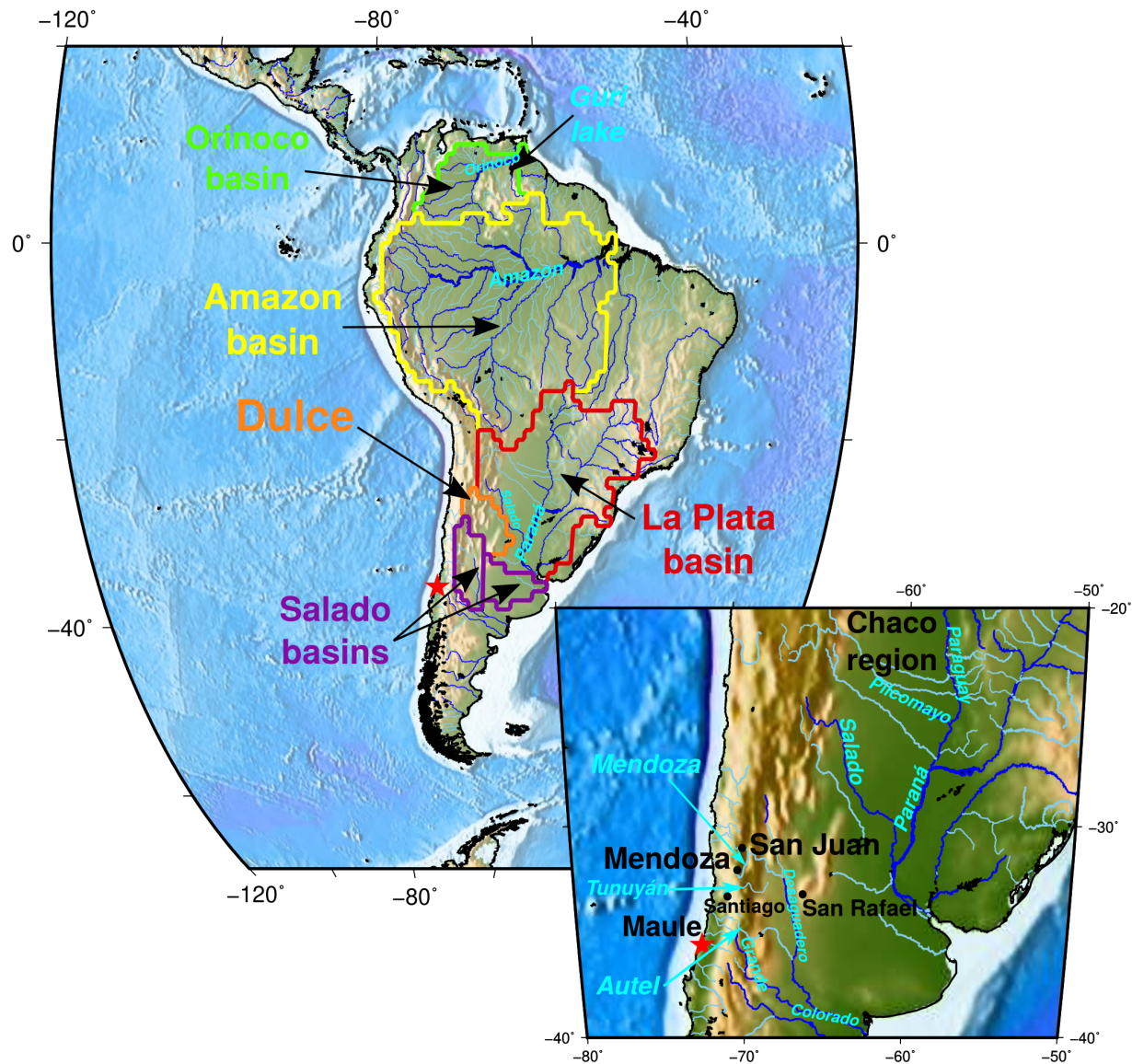


Figure S7: Map of the hydrological drainage basins in South America. The rivers names are written in blue, cities and regions in black.

## G Non-seasonal variability of the hydrological models

### G.1 6 months period before the earthquake

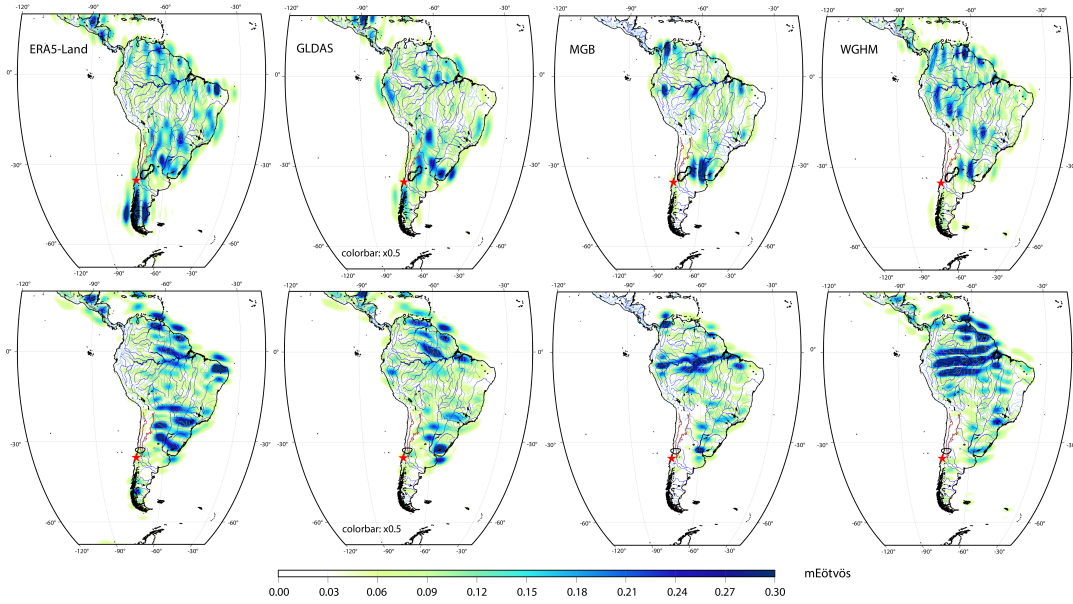


Figure S8: Spatial patterns of the non-seasonal signals in the gravity gradients from the ERA5-Land, GLDAS, MGB and WGHM hydrology models, as expressed by the rms of the 2009/09 – 2010/02 time series of gravity gradients at the scale 500-km (top line:  $\phi\phi$  gradients in the local spherical frame, emphasizing North-South oriented signals; bottom line:  $\theta\theta$  gradients, emphasizing East-West oriented signals). The annual, semi-annual and long-term trend components have been removed. Black lines, top panels: 0.15 mEötvös contour of the GRACE GRGS anomalous signal before the Maule earthquake shown in Main Fig. 3d. Black lines, bottom panels: 0.1 mEötvös contour of the GRACE GRGS East-West oriented anomalous signal in February 2010. Due to a high level of East-West elongated artefacts in the  $\theta\theta$  gradients at the 500-km scale, it is approximated by the contour of the  $\theta\theta$  gradients after a 30° clockwise rotation of the spherical frame.

## G.2 2003-2009 period

Over the 2003-2009 period, in the 500-km scale gravity gradients, the modelled hydrological signals remain very low (Fig. S9). In large basins as the Amazon and La Plata, this can be due to a different characteristic scale of the signals (larger than 500-km). See Section H.3 for a discussion of the ERA5 signal near the epicenter in the  $\phi\phi$  gradients.

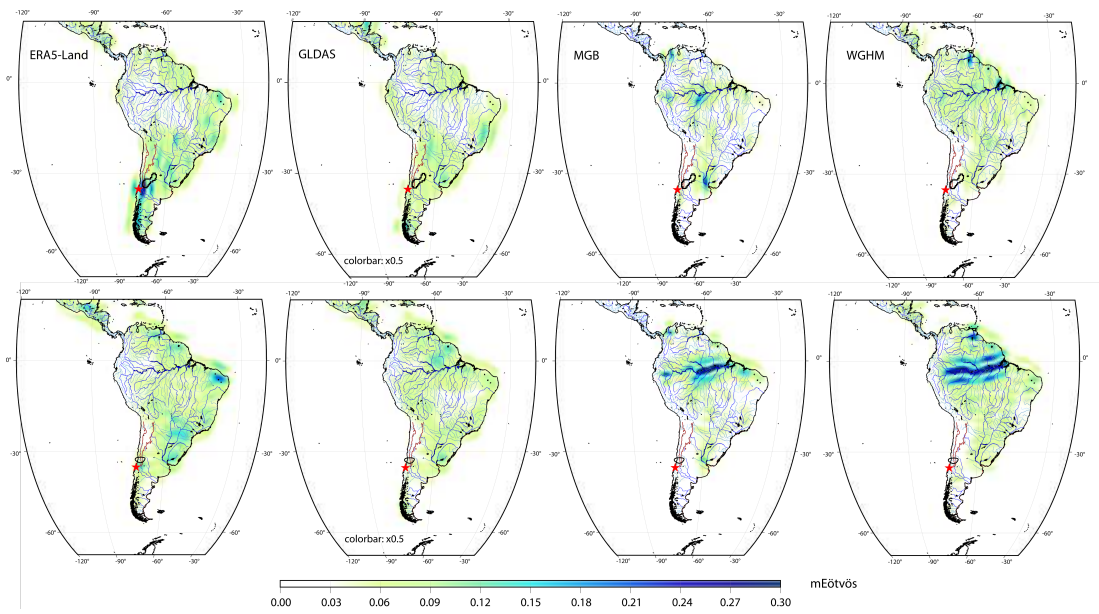


Figure S9: Same as Fig. S8, for the period 2003/01 – 2009/12.

### G.3 The seasonal cycle in ERA5-Land

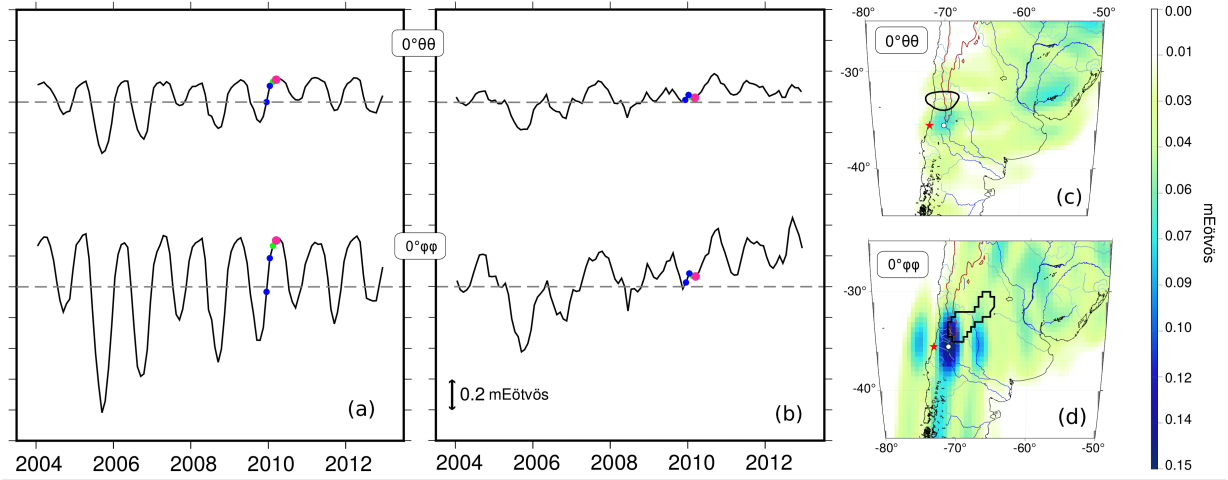


Figure S10: Time series and RMS maps over the 2003/01 – 2009/12 period, for the 500-km scale gravity gradients in the local spherical frame, computed from the ERA5-Land hydrological model. Panel a (resp. b): time series before (resp. after) correction for the annual and semi-annual cycles over the 2003/01 – 2008/12 period for the  $\theta\theta$  (top) and  $\phi\phi$  (bottom) gravity gradients. Panel c,d: RMS maps after correction for the annual and semi-annual cycles, for the  $\theta\theta$  (panel c) and  $\phi\phi$  (panel d) gravity gradients.

When comparing the hydrological models, we noticed differences between ERA5 and the other models. The ERA5 water storage amplitude appeared about twice larger than that of all the other models, hence the scaling by a factor of 0.5 applied for comparisons. In the Andean Cordillera close to the Maule region, contrary to the other hydrological models, the amplitude of its annual cycle varies irregularly by a factor up to 2.5 in the North-South gravity gradients, making the seasonal correction difficult (see Figure S10). This is why the RMS map of ERA5 in Fig. S8e comprises a small signal near Maule in the North-South direction (also present in the 2003-2009 period, see Appendix Fig. S9). Nevertheless, this contribution cannot explain the GRACE anomaly before the earthquake due to different spatial and temporal patterns. The geometry of this ERA5 indeed follows the topographic reliefs of the Andes, leading to an absence of signal in the East-West direction and at the larger 800-km scale in the North-South direction. In addition, its time evolution is roughly periodic.

## H Observed vs predicted anomalous February 2010 signals over South America

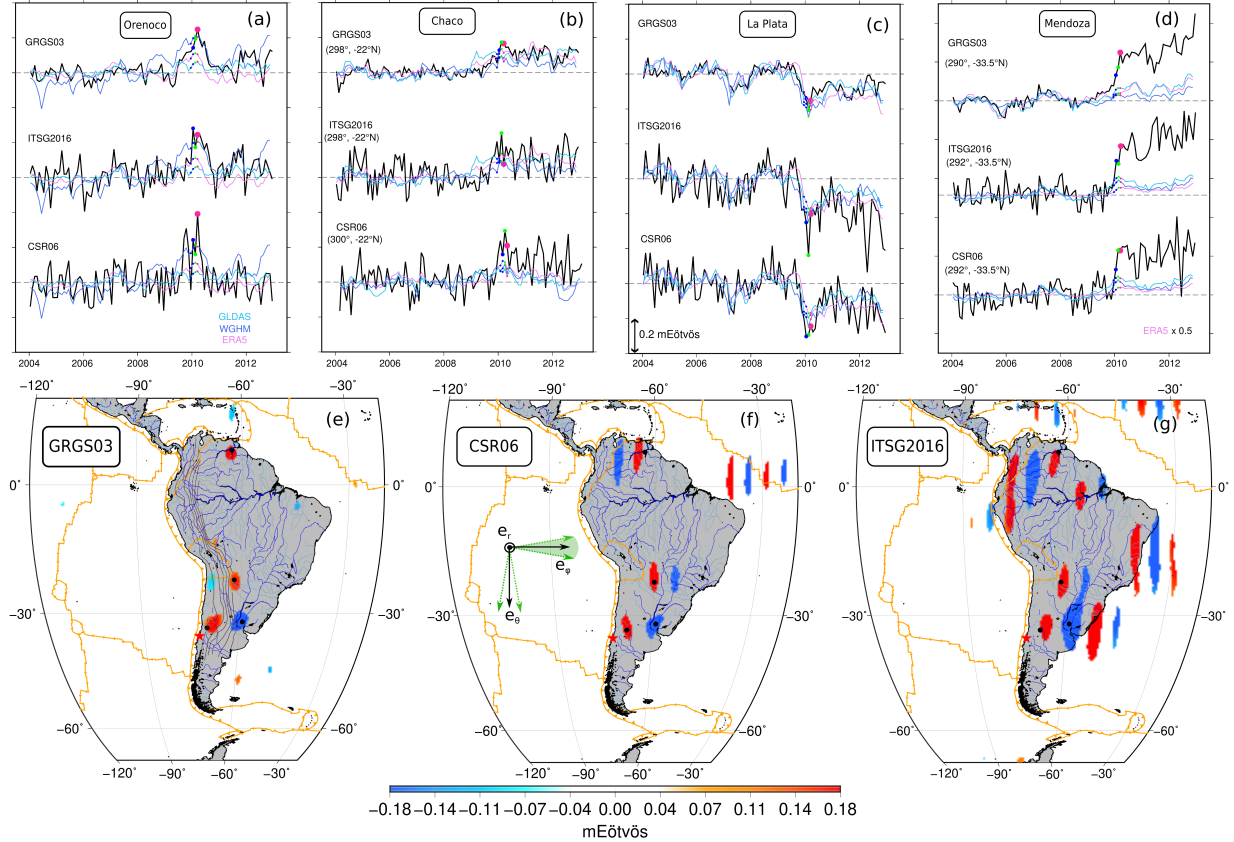


Figure S11: Anomalous signals in February 2010 in different GRACE solutions, without any hypothesis on a step-like evolution of the time series, compared with the predictions of hydrological models. Bottom panels e-g: maps of anomalous 800-km scale,  $\phi\phi$  gravity gradients in the local south-east-up spherical frame, emphasizing North-South oriented signals, for each GRACE solutions in February 2010 (GRGS: panel e, CSR: panel f and ITSG-2016: panel g). The anomalous February 2010 signals shown in these maps are those outside the [1-99%] percentile range of the long-term residual time series  $g(t)$  (see Section 2.4) for the CSR solution, outside the [2.5-97.5%] percentile range for the ITSG-2016 solution, and outside the [2.5  $10^{-5}$  - 99.99975%] percentile range for the GRGS solution. Top panels a-d: time series of the GRACE gravity gradients (black) and the predicted gravity gradients from three hydrological models (colors) for the same scale and orientation as in the maps e-g. The time series are given at the locations of the signals common to the three GRACE solutions in February 2010: a) Orenoco river ( $8^{\circ}N, 297^{\circ}E$ ), b) Pilcomayo river ( $22^{\circ}S, 298^{\circ}E$ ), c) La Plata ( $32^{\circ}S, 301^{\circ}E$ ) and d) Mendoza ( $33.5^{\circ}S, 290^{\circ}E$ ). These locations are marked by black dots on the maps.

# I Observed vs modelled co-seismic signal

Layer	Depth (km)	$V_P$ (m.s <sup>-1</sup> )	$V_S$ (m.s <sup>-1</sup> )	$\rho$ (kg.m <sup>3</sup> )
1	0 – 70	6700	3870	2900
2	70–	8000	4620	3400

Table 1: Earth model parameters for the modelling of the gravity gradient signals associated with the co-seismic rupture and the pre-seismic normal faulting.

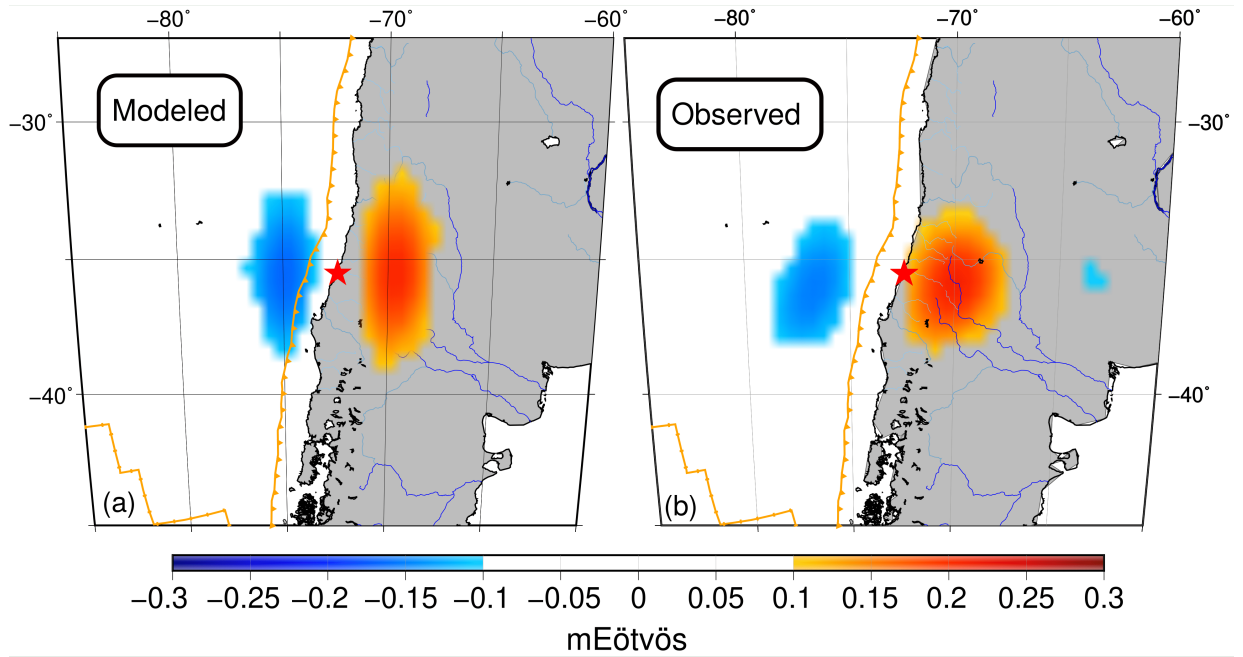


Figure S12: Comparison between the modeled and the GRACE-observed co-seismic gravity gradient signal (scale 800-km,  $\phi\phi$  gravity gradients in the local south-east-up spherical frame). Panel a: gravity gradient signal predicted from the co-seismic slip model by [27] (based on the spherical harmonics expansion of the corresponding geoid signal up to degree/order 60). Panel b: co-seismic step estimated in the GRACE GRGS gravity gradients in March 2010 (same as Main Fig. 1d)